Investigation of the summer Kara Sea circulation employing a variational data assimilation technique

G. Panteleev,[1] A. Proshutinsky,[2] M. Kulakov,[3] D. A. Nechaev,[4] and W. Maslowski[5]

Received 24 May 2006; revised 6 December 2006; accepted 26 January 2007; published 6 April 2007.

[1] The summer circulations and hydrographic fields of the Kara Sea are reconstructed for mean, positive and negative Arctic Oscillation regimes employing a variational data assimilation technique which provides the best fit of reconstructed fields to climatological data and satisfies dynamical and kinematic constraints of a quasi-stationary primitive equation ocean circulation model. The reconstructed circulations agree well with the measurements and are characterized by inflow of 0.63, 0.8, 0.51 Sv through Kara Gate and 1.18, 1.1, 1.12 Sv between Novaya Zemlya and Franz Josef Land, for mean climatologic conditions, positive and negative AO indexes, respectively. The major regions of water outflow for these regimes are the St. Anna Trough (1.17, 1.21, 1.34 Sv) and Vilkitsky/Shokalsky Straits (0.52, 0.7, 0.51 Sv). The optimized velocity pattern for the mean climatological summer reveals a strong anticyclonic circulation in the central part of the Kara Sea (Region of Fresh Water Inflow, ROFI zone) and is confirmed by ADCP surveys and laboratory modeling. This circulation is well pronounced for both high and low AO phases, but in the positive AO phase it is shifted approximately 200 km west relatively to its climatological center. During the negative AO phase the ROFI locaion is close to its climatological position. The results of the variational data assimilation approach were compared with the simulated data from the Hamburg Shelf Ocean Model (HAMSOM) and Naval Postgraduate School 18 km resolution (NPS-18) model to validate these models.

Citation: Panteleev, G., A. Proshutinsky, M. Kulakov, D. A. Nechaev, and W. Maslowski (2007), Investigation of the summer Kara Sea circulation employing a variational data assimilation technique, *J. Geophys. Res.*, *112*, C04S15, doi:10.1029/2006JC003728.

1. Introduction

[2] The general surface circulation pattern of the Kara Sea is shown in Figure 1. This ''classic'' circulation scheme has been reproduced in numerous publications [e.g., *Pavlov and Pfirman*, 1995; *Volkov et al.*, 2002] (and others) but was published first by *Berezkin and Ratmanov* [1940] based on historical ship and ice drift information. The circulation of the Kara Sea below the surface is poorly known but some data are available from moorings and ADCP (Acoustic Doppler Current Profiler) measurements. Approximately 50 moorings were deployed between 1956–1991 along the southern coast of the Kara Sea primarily for navigation needs. During the last two decades, 25 moorings were deployed in the central and northwestern parts of the Kara Sea. These observations were analyzed by *King et al.* [1996], *Loeng et al.* [1997] and *Scherbinin* [2001].

[3] The ADCP measurements were summarized for 1993–1996 by *King et al.* [1996], and *McClimans et al.* [2000] (hereafter McC00) and are shown in Figure 2. Interestingly, the major features of the measured circulation from Figure 2 disagree with currents presented in Figure 1. There are several reasons for this. First, although the circulation pattern of Figure 1 is known since the 1970s, it is based on observations before the 1940s. Circulation patterns derived relatively recently can be different from the classic circulation because of climate change (e.g. changes in wind forcing, ice coverage, river runoff). Second, the original pattern [*Berezkin and Ratmanov*, 1940] reflected not only summer data, but also information from other seasons so must be taken with caution. Third, there is much more data in our data archives now than was available for *Berezkin and Ratmanov* [1940].

[4] For this paper, we have compiled velocity data from a number of different sources (published figures and tables, and information from several declassified Arctic and Antarctic Research Institute data sets). Unfortunately, because of the relatively short mooring records, most of the data were averaged weekly and cannot be treated as robust characteristics of the summer circulation but some useful information for model validation in several regions could still be obtained.

[1] International Arctic Research Center, University of Alaska Fairbanks, Fairbanks, Alaska, USA.
[2] Woods Hole Oceanographic Institution, Woods Hole, Massachusetts, USA.
[3] Arctic and Antarctic Research Institute, St. Petersburg, Russia.
[4] Department of Marine Science, University of Southern Mississippi, Stennis Space Center, Mississippi, USA.
[5] Department of Oceanography, Naval Postgraduate School, Monterey, California, USA.

0148-0227/07/2006JC003728$09.00

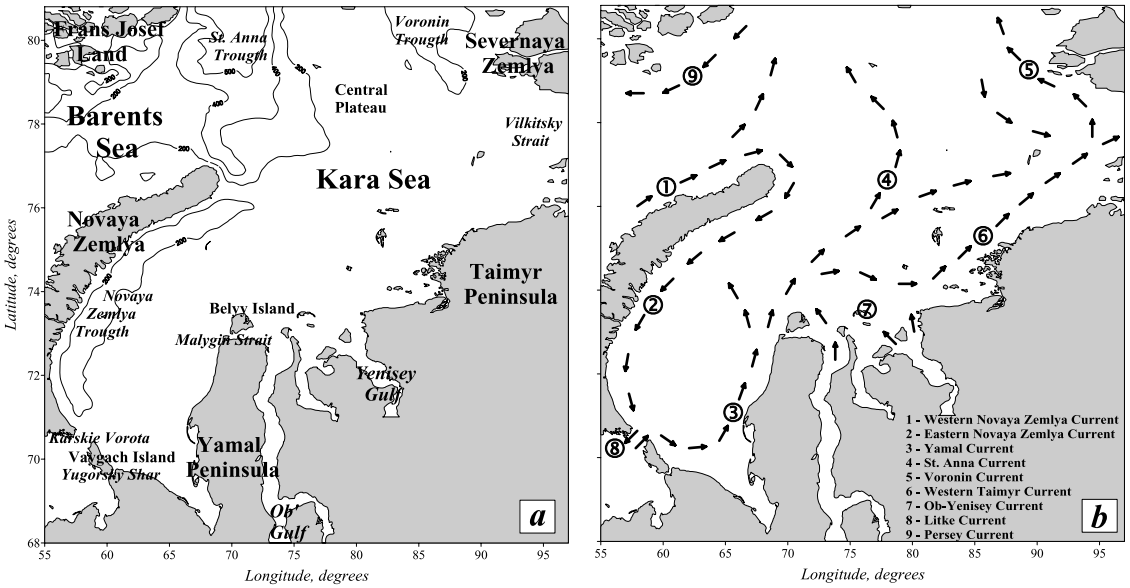

Figure 1. (a) The Kara Sea model domain and bathymetry (m). (b) The classic Kara Sea surface summer circulation pattern (adapted from *Soviet Arctic* [1970]).

[5] On the other hand, the existing observational information is not enough for serious and robust conclusions about the Kara Sea circulation not only in the deep layers but also at the surface due to sparse data and significant temporal and spatial variability of the currents. In this situation, numerical modeling is one of the appropriate tools to compensate for observational gaps.

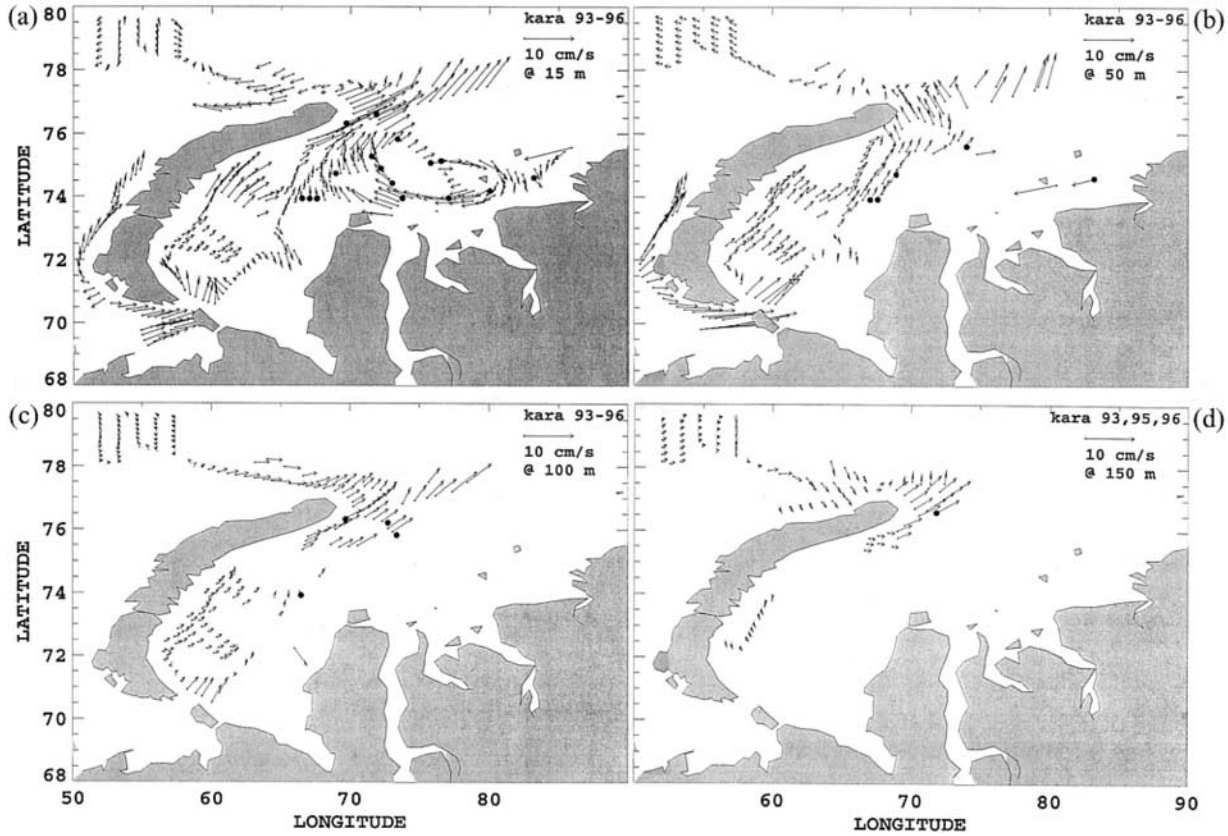

Figure 2. Late summer circulation vectors, composited from ADCP and moored current meters using data from 1993–1996: (a) 15, (b) 50, (c) (100), and (d) 150 m depth (adapted from *McClimans et al.* [2000]).

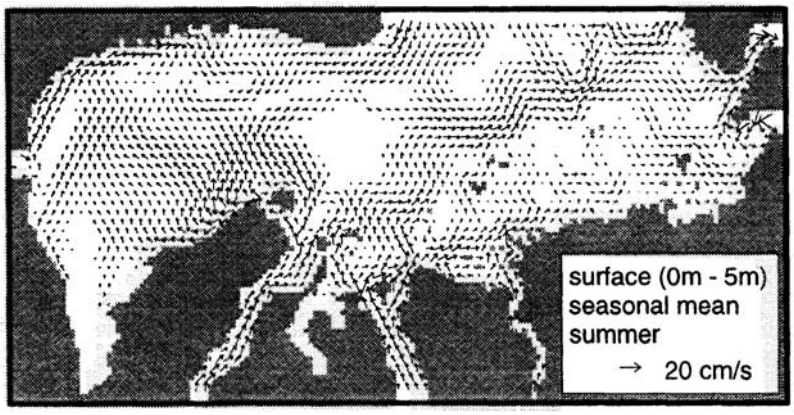

Figure 3. Simulated climatological summer 0–5 m layer circulation in the Kara Sea adopted for this publication from HK99.

[6] The first numerical studies of the Kara Sea were conducted by *Doronin* [1983, 1987] and *Doronin et al.* [1991]. They simulated circulations for different seasons and years based on atmospheric forcing and observed T and S fields employing relatively simple diagnostic barotropic and baroclinic numerical models. These studies showed that the circulation of the Kara Sea is influenced by different factors and that the circulation changes significantly from season to season and from year to year depending on the prevailing forcing. Among forcing parameters, wind, water exchange with the Barents Sea and the Arctic Ocean, and river runoff were identified as governing.

[7] *Volkov et al.* [2002] provided another diagnostic study of the Kara Sea circulation based on hydrographic surveys in August of 1977, 1978 and 1980. Some known features of the Kara Sea circulation from Figure 1 were reproduced very well but the interannual variability of simulated patterns for these years was significant, and circulation patterns for different years differed from the pattern in Figure 1.

[8] McC00 studied the circulation of the Kara Sea with a rotating laboratory model forced by climatological water transports at the open model boundaries and by river discharge. Despite many model simplifications, the McC00 results agree very well with observations. Trajectories of water particles reproduced by this model (Plate 2 from McC00) clearly indicate both an anticyclonic circulation in the central Kara Sea and a flow along the eastern flank of the Novaya Zemlya Trough (NZT).

[9] A more detailed numerical study of the Kara Sea circulation was carried out by *Harms and Karcher* [1999, 2005] (hereafter HK99 and HK05). The circulation was simulated with a high resolution (9.4 km) prognostic Hamburg Shelf Ocean Model (HAMSOM) [*Backhaus*, 1985]. The model was forced by seasonal atmospheric climatology, water, salt and heat fluxes, and by tides. The summer water circulation in the upper 5-m layer is shown in Figure 3. Comparing Figure 3 with Figure 2 reveals several differences. Among them is the absence of an anticyclonic circulation in the central part of the Kara Sea - the Region of Fresh Water Inflow (ROFI zone). Instead, the fresh water from the Ob and Yenisey rivers flows northward and eastward.

[10] Some information about the Kara Sea circulation could be extracted from the results of the Arctic Ocean Model Intercomparison Project (AOMIP) but AOMIP regional and global models do not really resolve the complex bathymetry of the Kara Sea and also they have to be validated against observations before use.

[11] One of the important problems of regional numerical modeling is that the regional model solutions strongly depend on the open boundary conditions which are usually highly uncertain. The accumulation of boundary condition errors may gradually deteriorate the solution of any numerical or laboratory model and cause disagreements with the observations. *Volkov et al.* [2002] demonstrated that a simple adjustment of boundary conditions can easily improve model results. But the question is how to adjust these boundary conditions correctly to satisfy observational data and to improve the model solution inside the model domain.

[12] The variational data assimilation approach [*Le Dimet and Talagrand*, 1986] provides an efficient way to achieve a better model-data agreement through the optimization of the model initial and boundary conditions. During the two last decades, this method was proved to be an extremely useful and efficient tool for the study of the ocean circulation [*Wunsch*, 1994; *Stammer et al.*, 2002; *Awaji et al.*, 2003]. This approach closes the gap between circulation studies relying heavily on observations (such as the dynamical method, water mass analysis and diagnostic modeling) and methods based upon dynamical constraints alone (such as prognostic model simulations).

[13] The major goal of this paper is to reconstruct a quasi-stationary circulation of the Kara Sea in summer. This circulation has to: a) agree with the observed hydrographic fields and velocities, and b) be dynamically balanced with forcing and internal parameters (to satisfy the dynamical constraints of a primitive equation model).

[14] To solve this problem, we have utilized a variational data assimilation approach proposed by *Tziperman and Thacker* [1989]. Their algorithm was successfully implemented by *Grotov et al.* [1998], *Yaremchuk et al.* [1998] and *Panteleev et al.* [2006b] in a number of studies of ocean circulation in different regions.

[15] Another goal of this publication is to show that the AOMIP models can be validated based on the results of

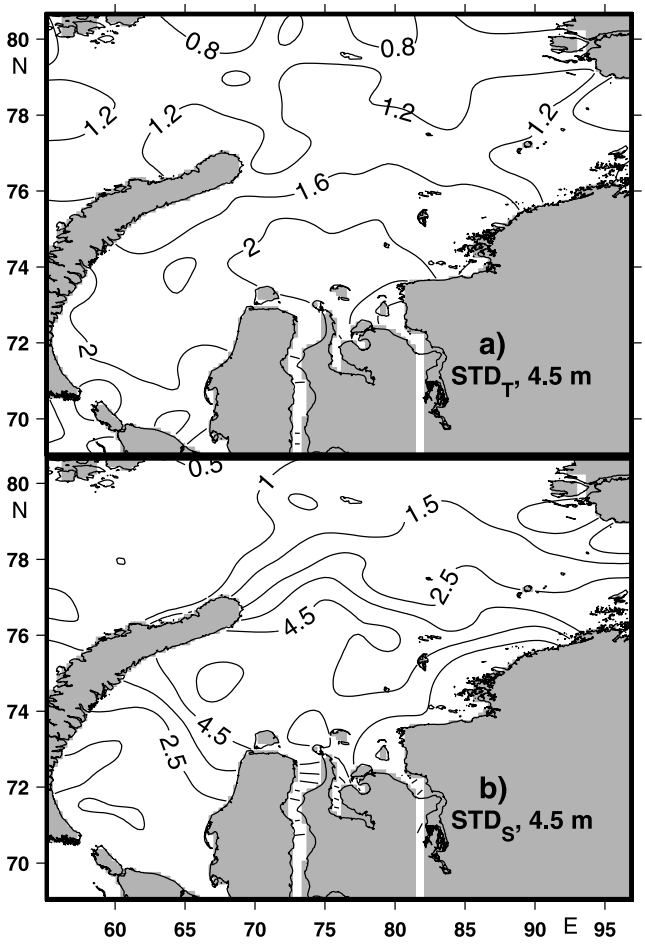

Figure 4. Standard deviation of the summer climatological T (°C, (a)) and S (ppt, (b)) data.

modeling with data assimilation. To estimate this possibility, the NPS-18 model results are used for analysis as an example of such an approach.

[16] This paper is organized as follows. Section 2 begins with a description of available data and their preliminary analysis. The numerical model, statistical hypotheses and specific details of the variational data assimilation procedure are outlined in section 3. In section 4, the major results of the reconstruction of the summer Kara Sea circulation are presented and are compared with observations and other models. Discussion and conclusions are provided in sections 5 and 6, respectively.

2. Data and Data Sources

[17] The procedure of the variational data assimilation techniques depends heavily on the data availability and quality, so it is logical to analyze the existing data first and then describe the data assimilation methods. The reconstruction of the summer circulation in the Kara Sea is based upon the following data sets: i) the summer climatological fields of T and S; ii) the mean summer wind stress and sea surface heat and salt fluxes; and iii) the estimates of total transports through the segments of the western open boundary. The data assimilation procedure prescribes relative weights to different parameters according to the reliability of observations. The observational data are accompanied by standard deviations (STD) for each parameter and are treated as characteristic of the data error. Variance takes into account both instrumental and interpolation errors. Signals of the processes not described by the model (e.g. interannual variability of the observations and data variability at weekly time scales) are also treated as data errors.

2.1. Hydrography

[18] Approximately 11,000 T and S summer profiles from 1930–2003 were extracted from *NOAA* [2004] and the Arctic and Antarctic Research Institute (AARI) database. Only data from August and September were used to avoid significant noise in water T and S fields associated with sea ice melt in June and July. The assimilation of the raw T and S profiles into the model is not computationally efficient since, in many cases, the individual profiles do not represent statistically independent climatological observations under the constraints of the model dynamics. In order to avoid this problem, the existing data were averaged for the period of the data reconstruction in the vicinity of each grid point. The number of T-S profiles in some model grid boxes was not sufficient to derive reliable estimates of data variance and for these cases, horizontal interpolation of the statistics characterizing data variability was carried out. The obtained climatological data and the estimates of the corresponding data STDs were used in the data assimilation procedure (Figure 4).

2.2. Meteorological Data

[19] The $0.5° \times 0.5°$ gridded wind stresses, heat and salt fluxes (evaporation minus precipitation, $E - P$) were extracted from the *DaSilva et al.* [1995], climatology. Figure 5a shows the mean summer wind stresses from this climatology. We have compared these data with wind stresses calculated from NCAR/NCEP sea level pressure reanalysis data and found very close agreement between these two data sets.

[20] The August–September mean $E - P$ vary from $1 \cdot 10^{-7}$ to $-4 \cdot 10^{-7}$ kg/m^2/s and do not change significantly from region to region in the Kara Sea.

2.3. Water Transports

[21] Kara Gate: Historical assessments [*Uralov*, 1960; *Turanov*, 1963; *Potanin and Korotkov*, 1988; *Loeng et al.*, 1993, 1997] show that the net inflow of the Barents Sea water into the Kara Sea via Kara Gate is approximately 0.5–0.6 Sv. This water transport was used by McC00 to simulate the Kara Sea circulation in their laboratory model. Recent direct measurements of the water transport in this region were conducted by *King et al.* [1996] using several day-long ADCP surveys in September 1995. Results of their measurements coincide with earlier studies and also show that the maximum current speed is approximately 20 cm/s.

[22] Observations from mooring during September 1997 [*Scherbinin*, 2001], show a persistent water flow from the Barents Sea to the Kara Sea with mean velocities approximately 5 cm/s in the vicinity of the Novaya Zemlya (NZ) and 26 cm/s near Vaigach Island. *Panteleev et al.* [2004] utilized these measurements in the analysis of volume, heat

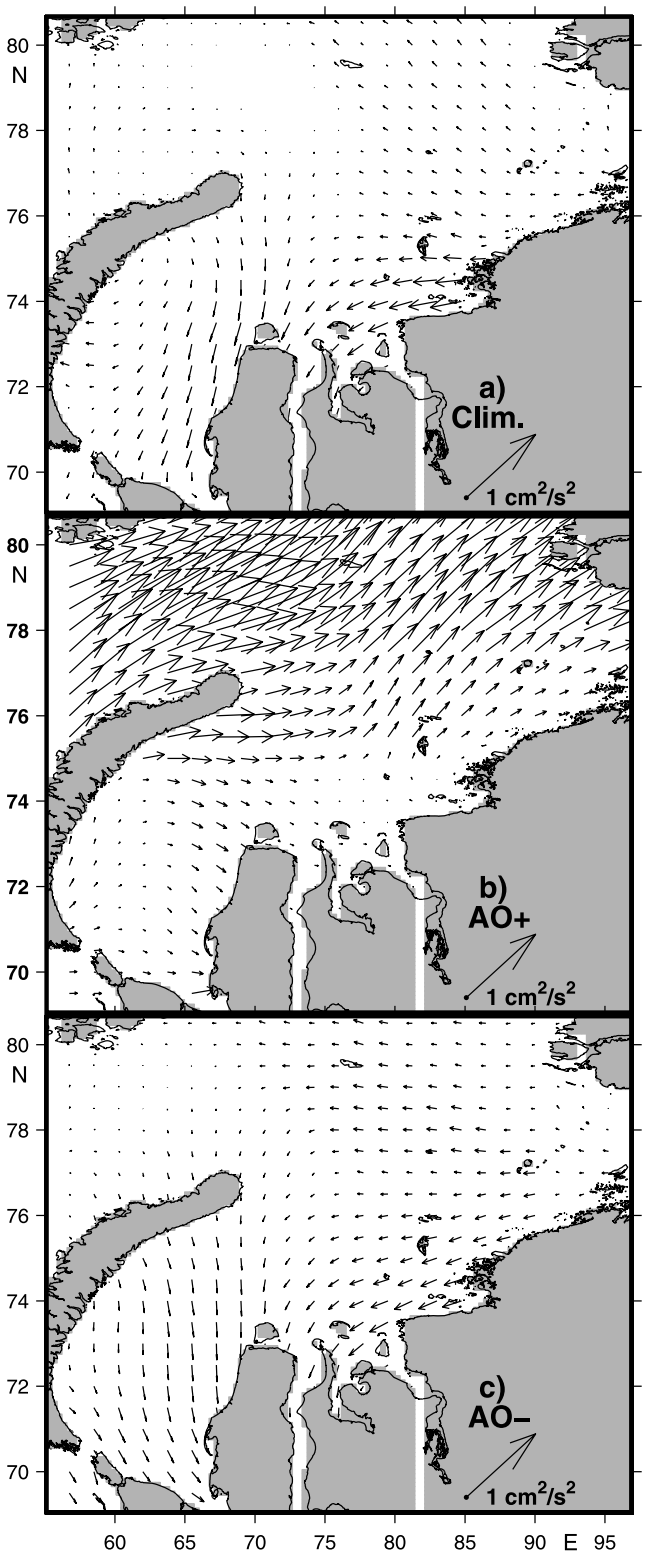

Figure 5. Summer wind stresses: (a) climatologic, (b) for AO positive and (c) for AO negative years.

and salt fluxes through the open boundaries of the Barents Sea with the application of simplified variational data assimilation section model. They found that the mean water transport via the Kara Gate has to be approximately 0.7 Sv in order to correctly explain and satisfy the structure of the velocity, T and S fields along the open boundaries. Taking into account these estimates, for this study it is assumed that the summer climatological water transport via the Kara Gate is 0.65 ± 0.2 Sv.

[23] Franz Josef Land (FJL) – Novaya Zemlya (NZ) passage: Information about water transport between the FJL and Cape Zhelania of NZ is rather controversial. The geostrophic calculations of *Uralov* [1960] and *Timofeyev* [1963] indicated that there is an inflow of the Barents Sea water to the Kara Sea of approximately 0.2–0.5 Sv, while *Loeng et al.* [1997] estimated this inflow as 1.6 Sv. This was based on the analysis of salt, heat and water volume balance in the Barents Sea. The only direct water transport measurements in this passage were reported by *Loeng et al.* [1993] from four moorings deployed for one year (1991–1992). The mooring records revealed a well-pronounced seasonal cycle in the water transport toward the Kara Sea, with net fluxes varying from 2.5 to 3.1 Sv in winter, and with an approximately 1 Sv flow in summer. Bearing in mind that the transport estimates based on mooring records do not consider the current along the FJL coast [*Loeng et al.*, 1993] and taking into account the indirect estimates discussed above, water transport of 1.05 ± 0.3 Sv was prescribed along this section for our study.

[24] Water transports via northern and eastern segments of the Kara Sea model domain (Figure 1) were not constrained to the observed fluxes because these data do not exist and the model has derived optimal water transports at these boundaries in order to satisfy model constraints for the other assimilated forcing and water parameters. The Ob and Yenisey river runoffs were adopted from *Pavlov and Pfirman* [1995] and prescribed as 0.02 Sv ± 0.005 for Ob river and as 0.015 Sv ± 0.005 for Yenisey. The water transports via different segments of the Kara Sea open boundary are summarized in Table 1.

3. Data Assimilation Technique

3.1. Forward and Adjoint Models

[25] To derive correctly the Kara Sea circulation from the data, the observational information has been combined with information imposed by the dynamical constraints. For this paper, the dynamical constraints are formulated as a numerical model based on a set of conventional primitive equations under Boussinesq and hydrostatic approximations. This model is a modification of the C-grid, *z*-coordinate OGCM designed in the Laboratoire d'Oceanographie Dynamique et de Climatologie [*Madec et al.*, 1999]. The model is implicit both for barotropic and baroclinic modes permitting model runs with relatively large time steps. The model is used in the "climatological" non-eddy-resolving mode on a relatively coarse grid with a 3-hour time step. A detailed description of the numerical scheme can be found in *Nechaev et al.* [2005] and *Panteleev et al.* [2006a].

[26] The model grid resolution is 0.1° along meridians and 0.35° along latitudes (approximately 10 × 10 km). The model bathymetry is from the ETOPO02 data set (http://www.ngdc.noaa.gov/mgg/fliers/01mgg04.html). There are 18 unequally spaced levels in the vertical direction with a resolution of 3 m near the surface and 50 m near the bottom of the deepest basins.

Table 1. Transports Via the Open Boundaries of the Kara Sea[a]

Boundary	From Literature, Sv	"Data," Sv	Optim. Climat., Sv
Ob	0.02	0.02 ± 0.005	0.018
Yenisey	0.015	0.015 ± 0.005	0.011
Kara Gate	0.4–0.7	0.65 ± .2	0.63
FJL-NZ	0.–1.6	1.05 ± .3	1.18
northern			1.32
eastern	0.6		0.52

[a]Left column: estimates taken from literature; central column: utilized as "data"; right column: optimized employing the variational data assimilation approach.

[27] The adjoint code of the model was constructed analytically by transposition of the operator of the tangent linear model, linearized in the vicinity of the given solution of the forward model [*Penenko*, 1981; *Wunsch*, 1996]. Application of the implicit scheme with large time steps results in a considerable reduction of storage requirements for variational data assimilation, since for nonlinear problems running the adjoint model requires storing the solution of the forward model every time step. The tangent linear model was obtained by direct differentiation of the forward model code. Therefore, the tangent linear and adjoint model are the exact analytical consequences of the forward model.

[28] In the course of data assimilation, the model solution is optimized by tuning free parameters (the so-called control vector) of the model. The control vector of the model is composed of values of the functions specifying initial conditions, open boundary conditions and surface fluxes. The set of initial conditions of the model includes the fields of sea surface height (SSH), T, S and horizontal components of velocity. Boundary components of the control vector comprise the distributions of T, S, and normal components of velocity specified on the open boundaries. The free-slip boundary condition for the tangent velocity component is set at the open boundary, therefore the values of the tangent velocity are not included in the control vector.

3.2. Cost Function

[29] The variational data assimilation can be formulated as a traditional least square problem [*Marchuk*, 1974; *Penenko*, 1981; *Le Dimet and Talagrand*, 1986; *Thacker and Long*, 1988]. The optimal solution of the model is found through constrained minimization of a quadratic cost function on the space of the model control vectors, where the cost function measures squared weighted distances between the model solution and data.

[30] Statistical interpretation of the least square method [*Thacker*, 1989; *Wunsch*, 1996] considers the cost function as an argument of the Gaussian probability distribution with the cost function weights being the inverse covariances of the corresponding data errors. Under the statistical interpretation, the optimal solution is the most probable model state for the given data realization and prior error statistics.

[31] Because of the sparseness of the oceanographic data and limited duration of the observational time series, practical data assimilation methods commonly rely on the assumption that the errors of different observations are δ-correlated [*Thacker*, 1989]. Under this assumption, the cost function weights are represented by the diagonal matrices, with diagonal elements being equal to the reciprocals of the corresponding data error variances.

[32] In the present study, we use the cost function $\mathcal{J}$, which, in addition to the "real" climatological data described in section 2, contains the so-called "bogus" data [*Thacker*, 1989] in the form of the smoothness and "stationarity" terms:

$$
\begin{aligned}
\mathcal{J} &= \mathcal{J}_C + \mathcal{J}_{\mathbf{u}} + \mathcal{J}_{stat} \\
\mathcal{J}_C &= \int_{\Omega,t} \left[W_C^{-1}(C - C^*)^2 + W_C^{s-1}(\Delta C)^2 \right] d\omega dt \\
&\quad + \int_{z=0} \left[W_B^{-1}(B - B^*)^2 + W_B^{s-1}(\Delta B)^2 \right] ds dt \\
\mathcal{J}_{\mathbf{u}} &= \sum_{n=1,N} W_{V,n}^{-1} \left(\int_{\Gamma_n} \int_{-H}^{0} \mathbf{u} dz d\gamma - V_n^* \right)^2 \\
&\quad + \int_{\Omega} W_{\mathbf{u}}^{s-1}(\Delta \mathbf{u})^2 d\omega dt \\
&\quad + \int_{z=0} \left[W_{\zeta}^{s-1}(\Delta \zeta)^2 + W_{\tau}^{-1}(\boldsymbol{\tau} - \boldsymbol{\tau}^*)^2 + W_{\tau}^{s-1}(\Delta \boldsymbol{\tau})^2 \right] ds dt \\
\mathcal{J}_{stat} &= \int_{\Omega,t} \left[W_{C_t}^{st-1} C_t^2 + W_{C_{tt}}^{st-1} C_{tt}^2 + W_{\mathbf{u}_t}^{st-1} \mathbf{u}_t^2 \right. \\
&\quad \left. + W_{\mathbf{u}_{tt}}^{st-1} \mathbf{u}_{tt}^2 + W_{\zeta_t}^{st-1} \zeta_t^2 + W_{\zeta_{tt}}^{st-1} \zeta_{tt}^2 \right] d\omega dt
\end{aligned}
\tag{1}
$$

[33] Here $\mathbf{u}$ denotes the horizontal velocity, ζ is sea surface height, $C = (T, S)$ is T and S, $\boldsymbol{\tau}$ is wind stress; B represents surface heat and salt fluxes, Γ_n denote the segments of the open boundary, V_n is the estimate of transport through the n-th segment of the open boundary, and $W_{\dots}$ are the variances of corresponding data. Asterisks denote the observed fields. The smoothness or "bogus" data terms in $\mathcal{J}$ are proportional to the squared Laplacians of the model fields. These terms were introduced into the cost function to regularize the data assimilation problem.

[34] Two groups of terms $\mathcal{J}_C$ and $\mathcal{J}_{\mathbf{u}}$ constrain baroclinic (T, S and heat/salt fluxes at the surface) and barotropic (SSH, velocity and wind stress) variables of the model, respectively. The physical meaning of the different terms in $\mathcal{J}_C$ and $\mathcal{J}_{\mathbf{u}}$ is straightforward: minimization of these terms enforces smoothness of the model solution and attracts it to the observed data. According to *Tziperman and Thacker* [1989], the third group $\mathcal{J}_{stat}$ ought to force the model solution to be quasistationary with a degree defined by weights $(W_{\dots}^{st})^{-1}$.

[35] The spatial and temporal distributions of "real" data variances $W_{\dots}$ were discussed in section 2. The variances of the "bogus" data are determined through the scale analysis: $W_C^s = C_s^2/L_C^4$, $W_B^s = B_s^2/L_C^4$, $W_{\mathbf{u}}^s = V_s^2/L_{\mathbf{u}}^4$, $W_{\zeta}^s = \zeta_s^2/L_{\mathbf{u}}^4$, $W_{\tau}^s = \tau_s^2/L_{\tau}^4$, $W_{Ct}^{st} = C_s^2/t_s^2$, $W_{Ctt}^{st} = C_s^2/t_s^4$, $W_{\mathbf{u}t}^{st} = V_s^2/t_{st}^2$, $W_{\mathbf{u}tt}^{st} = V_s^2/t_{st}^4$, $W_{\zeta t}^{st} = \zeta_s^2/t_{st}^2$, $W_{\zeta tt}^{st} = \zeta_s^2/t_{st}^4$, $t_{st} = 6$ months. The scales $V_s = 5$ cm/s and $\zeta_s = 10$ cm are defined as typical variations of these variables in the first guess solution, while the parameters C_s^2, B_s^2, τ_s^2 are derived from the characteristic spatial variability of the corresponding data. We utilized a uniform spatial scale for the wind stress fields $L_{\tau} = 500$ km, while spatial scales L_C and $L_{\mathbf{u}}$ are the

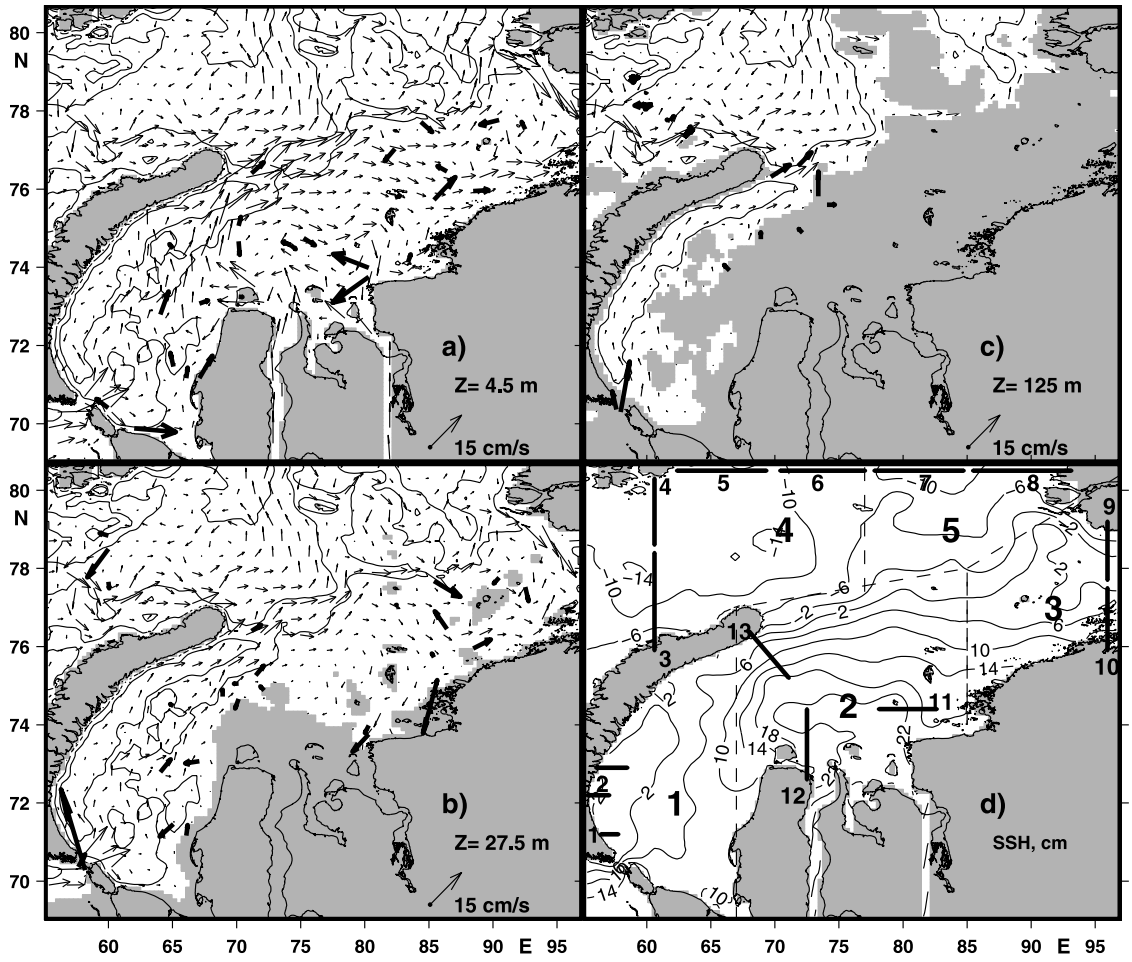

Figure 6. Reconstruction results. Optimized currents at (a) 4.5 m, (b) 27.5 m, and (c) 125 m depth. Thick arrows depict available velocity measurements. Sea surface heights (cm) are shown in Figure 6d). Dashed lines in Figure 6d depict boundaries between five regions of the Kara Sea shown by numbers 1, 2, 3, 4 and 5 in bold font. Thick lines with numbers denote sections where water transports were calculated (see also Table 2).

functions of the local depth gradient and vary within the ranges 100–300 km and 50–150 km respectively. This setting of the characteristic scales allows us to avoid oversmoothing of the model solution in regions with strong topographic steering.

[36] The procedure of the first guess initialization and the technique of sequential minimization of the cost function $\mathcal{J}$ are outlined in *Panteleev et al.* [2006a]. Starting with some prior estimate of the model control vector the model run is performed to obtain the first guess solution. Given the solution of the forward model the value of the cost function $\mathcal{J}$ is computed and the adjoint model backward is simulated in time to estimate the gradient of the cost function with respect to the control vector. The gradient of the cost function is then used in the quasi-Newtonian optimization algorithm [*Gilbert and Lemarechal*, 1989] to find a better estimate of the control vector of the model. The procedure is repeated until the norm of the cost function gradient is sufficiently small.

[37] Because of the model's nonlinearity, the cost function $\mathcal{J}$ may have multiple local minima. The quasi-Newtonian optimization algorithm finds only one local minimum, which is the closest to the first guess solution. The procedure of the first guess initialization and gradual minimization of cost function $\mathcal{J}$ is outlined in *Panteleev et al.* [2006a].

4. Reconstruction Results

[38] Theoretically, the reconstructed summer circulation and hydrography fields obtained by employing the variational data assimilation technique represent the most probable state of the Kara Sea conditions derived from the existing data. In this section, the reconstructed fields are described and the circulation parameters are compared with direct measurements, classic circulation schemes and with results from the models.

4.1. Comparison With Observations

[39] The optimized velocity and SSH fields are shown in Figure 6. Thick arrows depict observed velocities. These data have not been assimilated into the model and were used

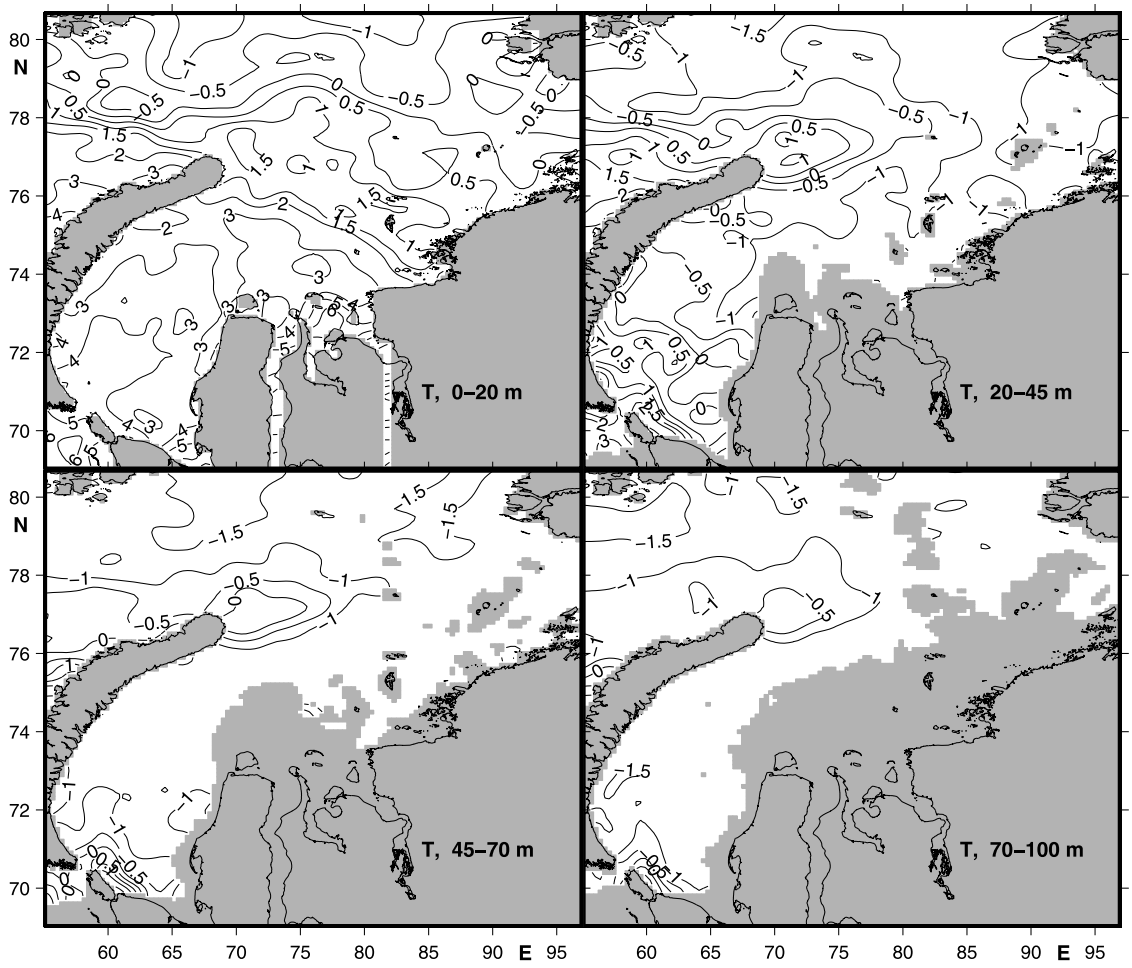

Figure 7. The optimized climatological T (°C) averaged for layers (a) 0–20 m,(b) 20–45 m, (c), 45–70 m, and (d) 70–100 m.

to validate the reconstructed results. Sections 1–13 are shown by thick black lines. Water transports through these sections calculated for different experiments are shown in Table 1. The water dynamics of the Kara Sea is analyzed here for five distinctive regions (see Figure 7d for region locations): (1) the western region with Novaya Zemlya Trough (NZT) (55°–67°E and 68°–77°N); (2) the central region or Region Of Fresh water Inflow (ROFI) (67°–85°E and 72°–77°N); (3) the eastern region (85°–95°E and 74°–78°N); (4) the northwest region, or St. Anna Trough (55°–77°E and 77°–81°N); and (5) the northeast region, or Voronin Trough (77°–95°E and 78°–81°N).

[40] Region 1: The currents of the upper 30 m layer in the southeast of this region (Figures 6a and 6b) resemble a cyclonic circulation pattern with a weak (≈1 cm/s) southwestward current along the NZ coast and a stronger (2–4 cm/s) northeastward branch along the eastern flank of the NZT. Velocities in deeper levels have a persistent northeast direction ranging from 1 to 3 cm/s (Figure 6c). The vertically integrated transport has a northeast direction and gradually increases from 0.07 Sv at section 1 to 0.13 Sv at section 2 (see section locations in Figure 6a) such that, as the southwestward current along the eastern NZ coast exists only in the upper layer and its influence on the total transport in the NZT is not significant.

[41] Our results do not show the Litke Current in the Kara Gate. The ADCP survey during September 1995 (Figure 2) and mooring observations in September 1997 [*Scherbinin*, 2001] also did not record the Litke Current in the Kara Gate. This current is a relatively narrow flow and likely has a baroclinic origin associated with a frontal zone separating fresh waters running from NZ to the sea and saline waters flowing to the Kara Sea via the Kara Gate. It is possible that this current is not revealed because the model is relatively coarse for this current horizontal resolution or because the resolution of climatological data is also too coarse to resolve this flow.

[42] Another interesting feature of the circulation in the NZT region is that the fresh water from the Ob and Yenisey rivers penetrates into the region and flows westward along Yamal Peninsula. Figure 6a (see also Figures 7a and 8a) shows that this flow then turns southward, reaches 72°N and deflects offshore as a north eastward current along the eastern flank of the NZT and joins the major branch of the Barents Sea water inflowing via Kara Gate. A similar flow pattern was observed in the McC00 laboratory model and in

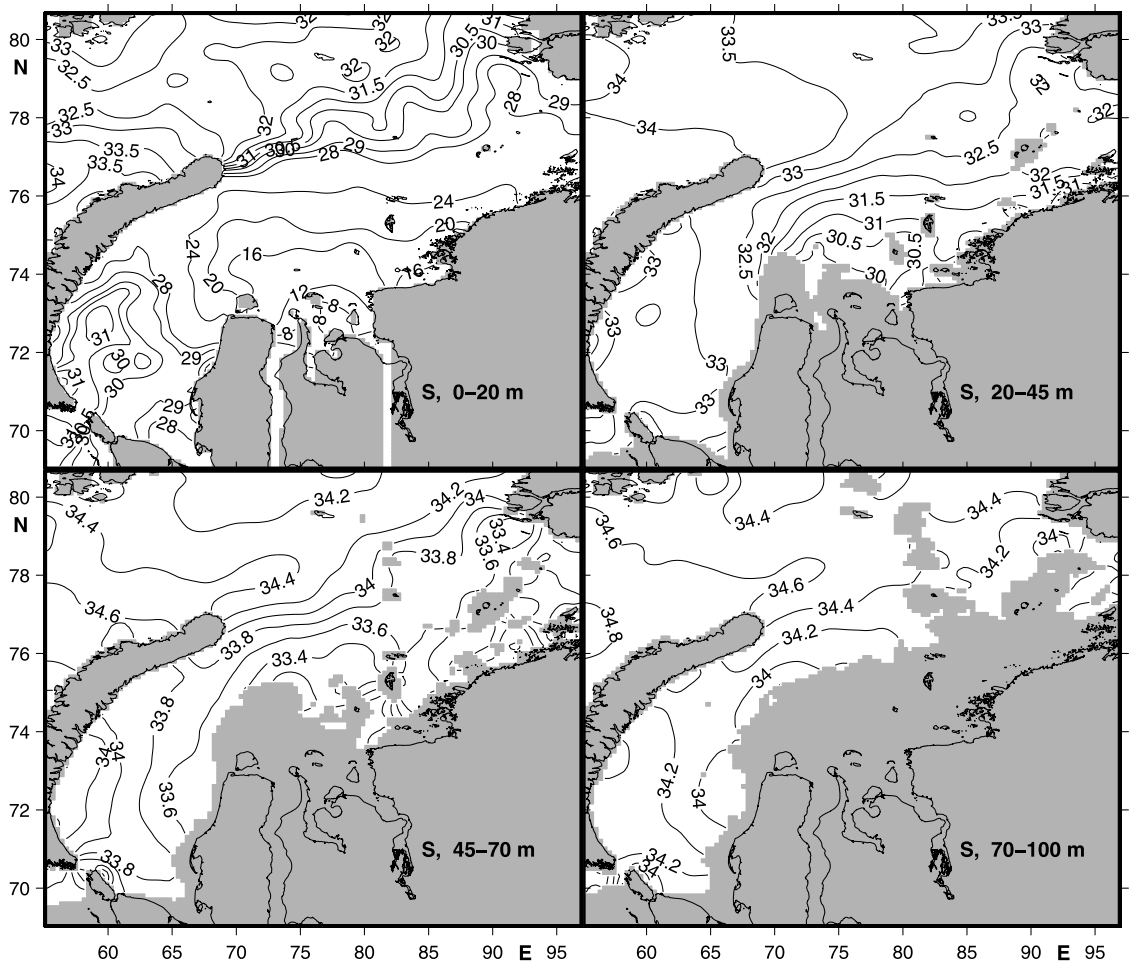

Figure 8. The optimized climatological S (*ppt*) averaged for layers of (a) 0–20 m, (b) 20–45 m, (c), 45–70 m, and (d) 70–100 m.

the numerical modeling results of the freshwater plume in the Kara Sea by *Kulakov and Stanovoi* [2002]. Figure 6 also shows that this current follows the steep slope of the NZT and gradually accelerates, reaching approximately 10 cm/s in the vicinity of section 13 with a total transport of 0.75 Sv through the section 13 shown in Figure 6d. The structure of this NZT through-flow is in good agreement with ADCP velocities (Figure 2) and with trajectories of 3 ice beacons reported by McC00.

[43] As it is seen from Figures 7 and 8, the relatively warm and saline Barents Sea water enters the Kara Sea via Kara Gate causing a T and S increase in the surface and deeper layers. Further downstream, the surface T gradually decreases from 5°C near Kara Gate to 1° near the northern tip of NZ. According to Figure 7, the T distribution in the layer 20–45 m reveals a thin strip of warm water along the NZ coastline. The modeled vertical velocity in this region (not shown) indicates downwelling, but the origin (wind forcing, for example) of this downwelling is not clear and additional experiments are needed for robust conclusions.

[44] Region 2: The T and S distributions in Figures 7a and 8a and velocity field in Figure 6a clearly indicate that the river discharge in this region forms an area of brackish and relatively warm waters with clockwise/anticyclonic rotation (Figure 6a).

[45] An anticyclonic circulation in the central part of the Kara Sea (ROFI) is a prominent feature of the reconstructed circulation, but the classic scheme in Figure 1 does not show this anticyclonic circulation cell. At the same time, the reconstructed velocity field agrees well with the mooring data and with the ADCP data in Figure 3. McC00 speculated that this remarkable circulation cell is generated by freshwater accumulation in the shallow ROFI zone during intensive river discharge in June and July. In August and September, the river discharge reduces and the ROFI freshwater pool acts as a zonal barrier deflecting river runoff to the left. It is interesting that water transport through section 12 is 0.09 Sv and is 3 times larger than the total river runoff. This means that the anticyclonic circulation driven by baroclinic effects in this region returns waters into the area. This is confirmed by estimates of water transport through section 11 (eastern branch of ROFI circulation) which is 0.08 Sv and is rather significant.

[46] The optimized S fields shown in Figure 8 also agree with the water circulation discussed above. S gradients and frontal zones observed in the upper layers of the Kara Sea

indicate that the summer circulation of the Kara Sea (when strong winds are absent) is density driven and is regulated by river discharge and water inflow from the Barents Sea.

[47] Region 3: The circulation pattern in region 3 is characterized by an eastward through-flow toward Vilkitsky and Shokalski straits and agrees with Figure 1. Another feature of this region is a week anticyclonic circulation around several islands. This disagrees with Figure 1 which shows more cyclonic type water rotation.

[48] The reconstructed water transports through Shokalsky and Vilkitsky Straits are shown in Table 1 and are indicated by sections 9 and 10, respectively. The total water transport to the Laptev Sea is estimated as 0.52 Sv. The Vilkitsky and Shokalsky straits play a very important role in the Siberian coastal water dynamics by allowing transportation of the Kara Sea waters eastward to the Laptev Sea and further east toward the Bering Strait.

[49] Region 4: The reconstructed circulation in region 4 generally agrees with Figure 1, revealing a strong water inflow via the NZ–FJL strait along the northern coast of NZ, and an outflow along the southern coast of FJL (which could be identified as the beginning of the Persey current, known more as a current of the northern Barents Sea) and an inflow/outflow along the western and eastern sides of the St. Anna Trough, respectively. The reconstructed optimized transports through sections 3 and 4 showing water dynamics associated with the St. Anna Trough, are presented in Table 1. Balancing water inflow via sections 3 and 4 (1.18 Sv) with transports through sections 5 and 6 (1.17 Sv) allows us to conclude that practically all water flowing to the Kara Sea between NZ and FJL flows out through the St. Anna Trough.

[50] Several velocity measurements observed at 125 m in 1992–1993 and 1997 (Figure 6c) confirm the reconstructed circulation fields at this level, but the reconstructed circulation in the upper layers disagrees significantly with the observations of McC00. McC00 analyzed this problem and concluded that the wind regime during their observations was not typical for summer conditions, resulting in water outflow from the Kara Sea instead of inflow. In the deep layers, at 100 m depth and below, the inflow pattern agrees with our reconstructed circulation scheme.

[51] The water from the Barents Sea flows in between the NZ and FJL as an intense current with velocities of 10–15 cm/s near the NZ coast (Figure 6). The current follows the 200 m isobath and deflects northward near the tip of NZ, presumably due to the sharp topography break. Thus, the currents along the western and eastern NZ coasts diverge in the vicinity of the northern tip of NZ. The outlined behavior of these currents allows warm water to be accumulated in the vicinity of the tip of NZ (Figure 7b). Recently, the presence of a relatively warm water (0.5°C up to 2.5°C) in this area was observed by *Pivovarov et al.* [2003].

[52] Region 5: The water circulation in this region is significantly influenced by the bathymetry of the Voronin Trough and reveals a weak inflow of the Arctic Ocean waters via section 7 (0.07 Sv) and a major outflow of the Kara Sea waters through section 8 (0.22 Sv).

[53] It is important to note that the variational data assimilation approach allowed us to reconstruct the circulation in the the St. Anna and Voronin Troughs without prescribing water transports through the northern and eastern boundaries, and only observed T and S fields assimilated into the model were used under the geostrophy and continuity constraints of the model dynamics.

[54] The S distribution (Figure 8) reveals a local S minimum in east part of the region 5, which coincides with minimum of monthly averaged ice concentration in this regions [*Volkov et al.*, 2002]. Probably, this feature is related to the intensive summer melting of sea ice that accumulates in the region due to prevailing currents and winds. This S minimum is responsible for an anticyclonic type of water motion in addition to the bathymetric dominating factor which governs the major circulation features in the Kara Sea. The ''classic'' circulation scheme in Figure 1 partially disagrees with the circulation discussed above.

4.2. Comparison With Model Results

4.2.1. Laboratory Model, McC00

[55] Reconstructed circulation results agree well with the circulation patterns of the McC00 laboratory model. Both studies cover common model domains and utilize more or less similar water transports through the Kara Gate, NZ–FJL passage and river discharge (see Table 1). As a result, the optimized Kara Sea circulation in the NZT and ROFI zone resembles trajectories of particles in the McC00 model (see Plate 2 from McC00). At the same time, both laboratory model and variational data assimilation results agree well with the ADCP-based circulation scheme in Figure 2.

[56] On the other hand, the optimized circulation pattern requires water inflow through sections 5 and 7 of 0.5 Sv that is half the transport prescribed in the McC00 laboratory model and some differences are expected between reconstructed fields and McC00 model results in this region.

4.2.2. Regional High Resolution Numerical HK99 Model

[57] The mean summer Kara Sea surface circulation pattern of HK99 (Figure 3) differs significantly from the reconstructed velocity fields.

[58] In region 1, the HK99 circulation shows an intensification of the currents along the east NZ coast in the southern part of the NZT (72°–74°N). As a result, the SSH derived by HK99 has a small maximum in the center of the NZT, while our results indicate a small minimum in the SSH distribution (Figure 6d) resulting in a weak southwestward current along the east NZ coast (Figure 6a). Despite the simple preprocessing method for the raw ADCP data and strong smoothing with a typical scale of 126 km, the composite ADCP velocities (Figure 2) show very weak currents along the east NZ coast near 72°N. Several other models [e.g., *Karcher et al.*, 2003] also do not reveal the intense northeast current along the east coast of NZ.

[59] In region 2, at the location of section 13, the HK99 model shows a strong inflow into the model domain (Figure 3). This agrees with the classic circulation scheme of the Kara Sea (Figure 1), but contradicts the available current meter data (Figure 6), ADCP survey results (Figure 2), and the local S distribution (Figure 8). The summer S distribution indicates a zonal front in this area (Figure 8a) but HK99 S fields do not have this feature because of several reasons associated with a weak imbalance between fresh water river runoff, salt fluxes due to ice melt and growth, and due to the transport of

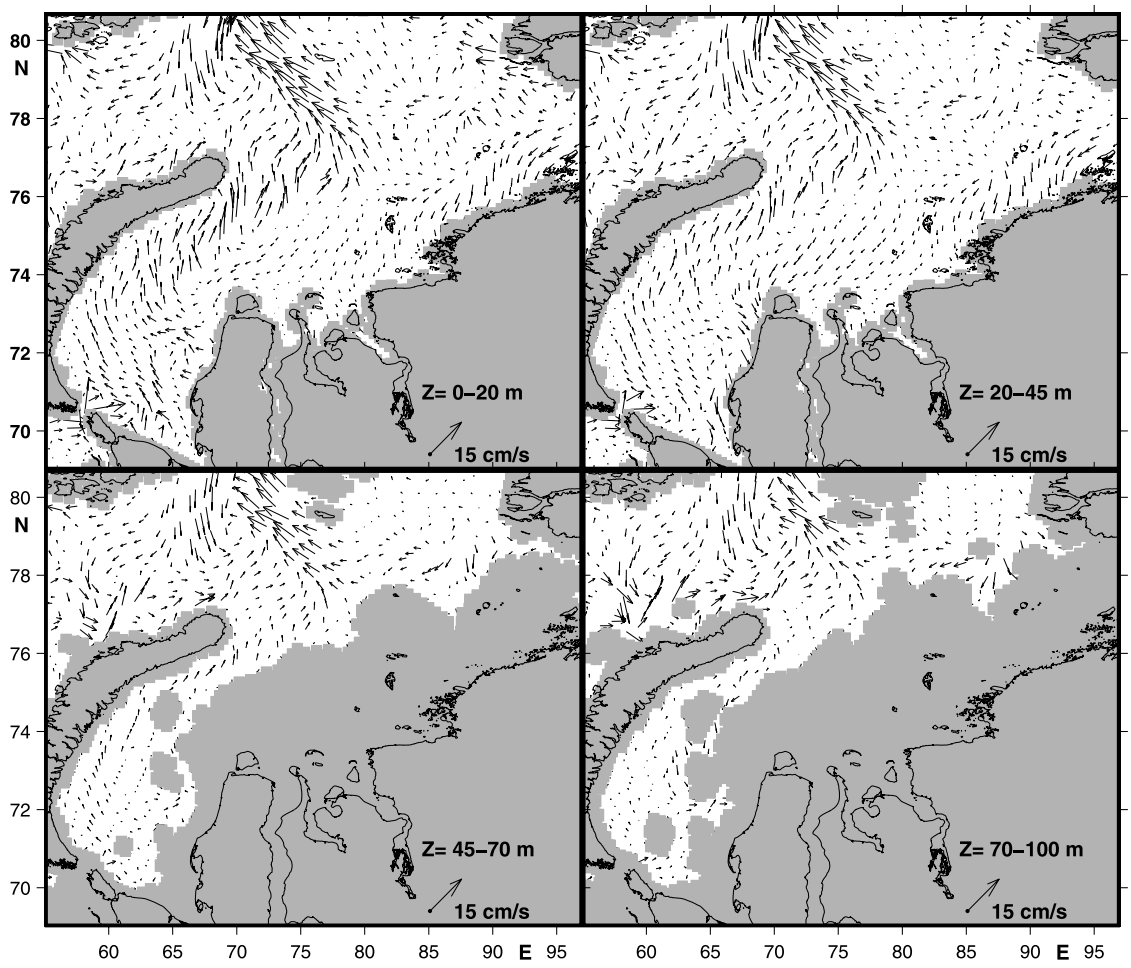

Figure 9. August–September circulation patterns from NPS-18 model results for layers of (a) 0–20 m, (b) 20–45 m, (c) 45–70 m, and (d) 70–100 m.

sea ice from the Kara Sea to the Arctic Ocean. The underestimate of freshening of the Kara Sea by this model was discussed by HK99 and is a known problem of this simulation.

[60] Third, the HK99 surface circulation in the ROFI zone is not so pronounced as in the optimized reconstructed fields and in the McC00 results. There are two relatively broad outflow areas formed by the Ob and Yenisey discharges shown in Figure 3 with zero currents in the vicinity of the ROFI zone. This is mostly because of the underestimation of water freshening in the Kara Sea by this model as discussed above.

[61] For the HK99 model results, our speculations are based on a simple visual analysis of the circulation patterns. Below, a more detailed examination provides some quantitative estimates of the differences between the reconstructed fields and fields extracted from the results of the Pan-Arctic regional ice-ocean coupled model of the Naval Postgraduate School.

4.2.3. Regional High Resolution Model of the Arctic Ocean

[62] Results of the Naval Postgraduate School regional coupled Arctic Ocean and sea ice general circulation model are available for the AOMIP investigators at ftp://ftp.arsc.edu/private/maslowsk/AOMIP. The ocean model is based on the GFDL formulation adapted for parallel computers [*Smith et al.*, 1992]. The rotated numerical grid covers the Arctic Ocean, the subpolar seas and the North Atlantic to approximately 50°N latitude. The Bering Strait is closed. No mass flux is allowed through the closed lateral boundaries. The grid is relatively fine (18 km and 30 levels). More details about the ocean model can be found in *Smith et al.* [1992].

[63] The ice model is a version of the *Hibler* [1979] viscous-plastic, dynamic-thermodynamic ice model, adapted for parallel computers. At the ice surface, heat flux is calculated according to the energy budget, as in *Parkinson and Washington* [1979]. ECMWF data have been used for the calculation of the energy budget and surface wind stress. Using this forcing, the model has been shown to give realistic distributions of sea ice properties [*Zhang et al.*, 1999].

[64] The 30-year model output consists of monthly parameters of three dimensional T, S and water velocity fields at 30 depth layers between limits: 0, 20, 45, 70, 100, 140, 180, 240, 300, 380, 460, 580, 720, 920, 1120, 1320,

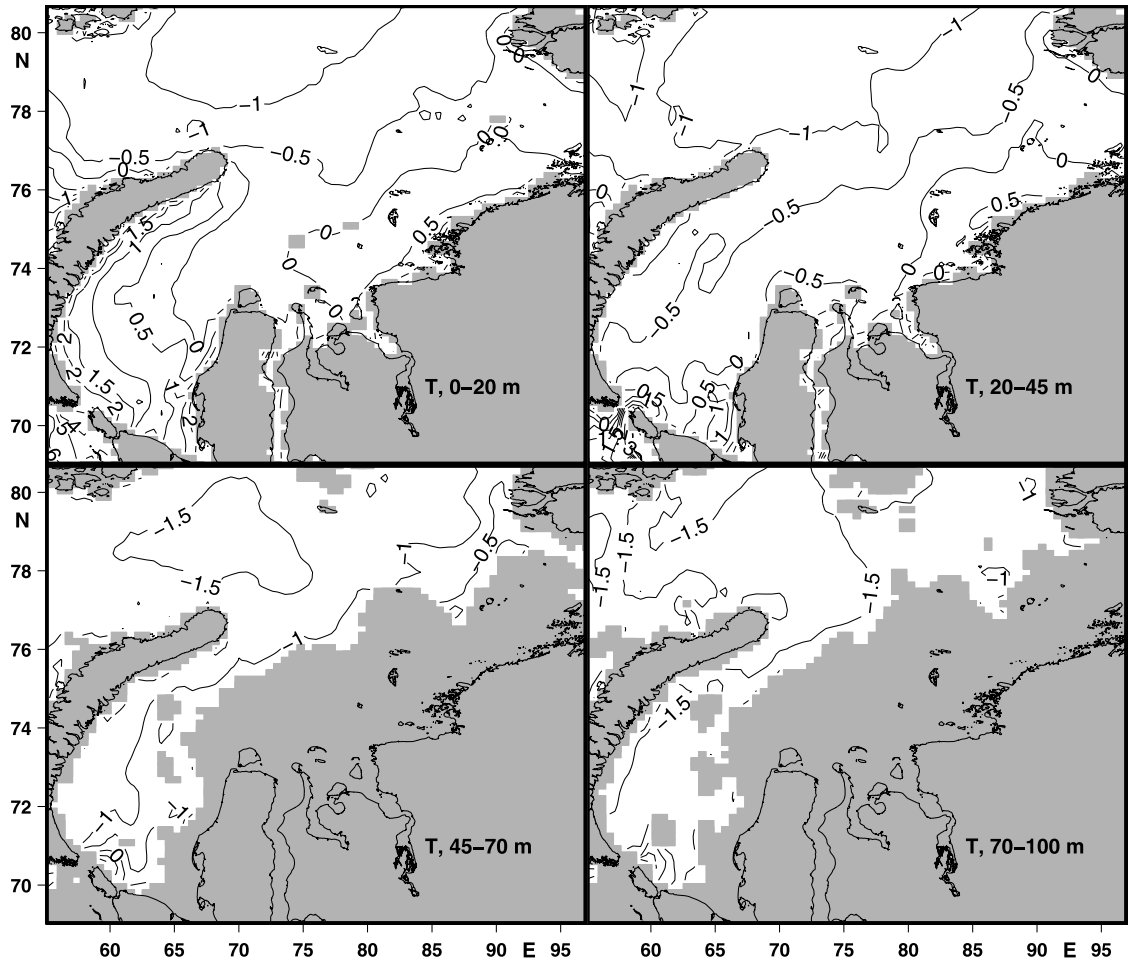

Figure 10. August–September water T fields from NPS-18 model results for layers of (a) 0–20 m, (b) 20–45 m, (c) 45–70 m, and (d) 70–100 m.

1520, 1720, 1920, 2120, 2320, 2520, 2720, 2920, 3120, 3320, 3520, 3720, 3920, 4120, and 4320 meters, such that the first layer is between 0 and 20 meters, the eighth layer is between 240 and 300 meters, etc. In order to compare the results of this model with the reconstructed fields, we averaged the reconstructed data for the layers of the NPS-18 model. Summer climatological currents, T and S fields in the original model grid are shown in Figures 9–11. Figures 12–14 show the differences between reconstructed fields and NPS-18 model results for currents, T and S in different layers, respectively.

[65] Both reconstructed and NPS-18 model solutions (Figures 6 and 9) reveal the southward current along the Yamal Peninsula, strong northeast flow along the eastern flank of the NZT, the eastward inflow in the southern part of the NZ–FJL passage, and outflow in its northern part. At the same time, there are significant differences in the magnitude of the velocities. The reconstructed velocities are stronger and the difference is well documented in Figure 12. The optimized velocities (Figure 6) in the Kara Gate and NZT are nearly twice as large as the velocities of NPS-18 model. On the other hand, the Persey Current is better represented by the NPS-18 model than in the reconstructed results. The NPS-18 currents in this region agree better with available observations (compare Figure 6 and Figure 9).

[66] There are significant discrepancies between the NPS-18 and reconstructed velocity fields in the other regions of the Kara Sea and these differences can be summarized as:

[67] (a) The NPS-18 circulation pattern (Figure 9) does not show the anticyclonic circulation in the central Kara Sea (ROFI zone). Instead, the NPS-18 solution indicates the broad westward flow along the Siberian coast which extends westward from the Vilkitsky Strait. The available ADCP measurements and mooring observation (Figures 2 and 6) do not support these results. The relative error $\varepsilon_u = (\sum_N (\mathbf{u} - \mathbf{u}^*)^2 / \sum_N \mathbf{u}^{*2})^{0.5}$ between the NPS-18 model and available velocity observations (thick arrows in Figure 6) ranges between 2 and 3 in the surface layer (0–40 m), while similar errors for the optimized velocity field (Figure 6) are about 0.8.

[68] (b) The NPS-18 model inflow via the Vilkitsky Strait contradicts the T and S fields and the well known phenomenon of the eastward freshwater transport along the Siberian coast.

[69] (c) There are also notable differences in the circulation in region 4. According to the NPS-18 circulation

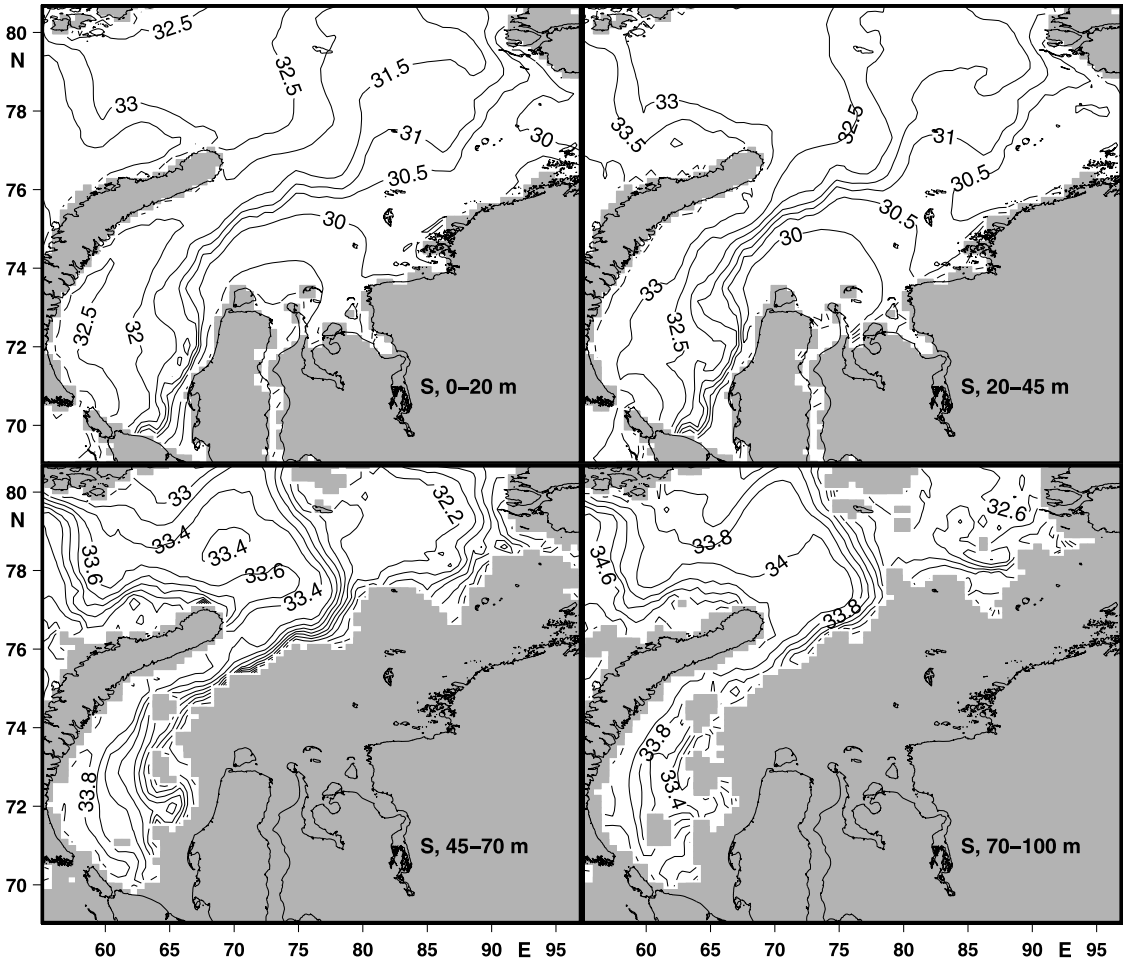

Figure 11. August–September water S from NPS-18 model results for layers of (a) 0–20 m, (b) 20–45 m, (c) 45–70 m, and (d) 70–100 m.

pattern (Figure 9), the major outflow of all waters coming to the Kara Sea occurs via St. Anna Trough. This disagrees with the observed zonal S and T fronts near the northern tip of NZ (Figures 7 and 8).

[70] Comparing T and S reconstructed fields with NPS-18 model results (see Figures 14 and 15) shows that the NPS-18 model water T is 3°C to 4°C lower than the reconstructed T in the surface layers of the river deltas and in the center of region 1, 1°C to 2°C lower than reconstructed along the eastern coast of NZ, and approximately 1°C lower in the other regions of the Kara Sea. In the deeper layers (20–45 m, 45–70 m) except for the region in the vicinity of Mys Zhelania, this difference changes sign and NPS-18 water T are higher than in the reconstructed T and S fields. Below 70 m, both models show good agreement except in the region of the NZ tip, where the reconstructed water T is approximately 1 degree higher than the NPS-18 model results. These T and S distributions show that vertical water stratification is not well reproduced by the NPS-18 model. Figure 15, where vertical water T and S profiles are presented for different regions, confirms this.

[71] Differences in the water salinities are even larger than in the water T between the modeling with data assimilation and the NPS-18 model. Figure 15 reveals that the S of NPS-18 model is much higher in the upper 0–20 m layer than the reconstructed S. This is especially pronounced in the river deltas where the difference reaches 15 S units. In the deeper layers, the NPS-18 salinities are less than the reconstructed salinities, indicating that the vertical water stratification in the NPS-18 model does not reproduce the thermocline and halocline in summer.

5. Discussion

[72] In this section we discuss some possible reasons for the disagreements between the reconstructed and simulated summer currents, and T and S fields in the Kara Sea.

5.1. Possible Causes of Model Differences

[73] In order to clarify reasons that cause the differences between the HK99 and the reconstructed circulation results, two numerical experiments were carried out. In the first experiment, the assimilation procedures described above ("control" model run) were repeated but water transport in the Kara Gate was reduced to 0.2 Sv. This mean summer transport via the Kara Gate was utilized by HK99. The major goal of this experiment was to investigate how changes in the Kara Gate inflow influence the circulation

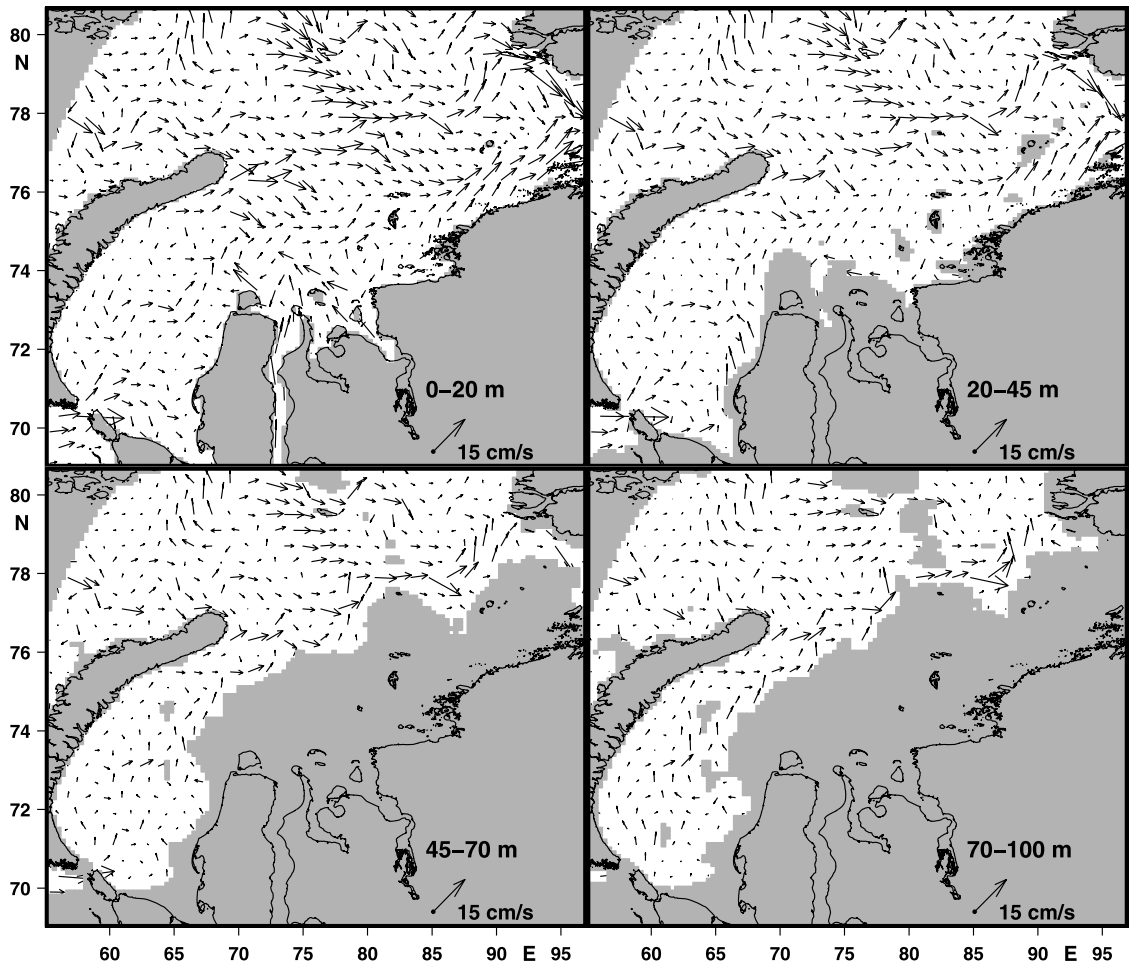

Figure 12. Differences between vectors of reconstructed currents and NPS-18 model results for layers of (a) 0–20 m, (b) 20–45 m, (c) 45–70 m, and (d) 70–100 m.

structure of the Kara Sea. In the second experiment, the Kara Gate transport was defined as 0.65 Sv as in the "control" model run, but the T and S fields were prescribed uniform without gradients in the vertical and horizontal directions (T = 5°C and S = 20 ppt in all grid points of the model domain). In this experiment we investigated how the absence of baroclinic effects influenced the circulation in the region.

[74] The surface circulation patterns for these experiments are shown in Figure 16. Comparing Figure 16a with Figure 6a shows an intensification of cyclonic circulation in the southern part of region 1. There are no more visible differences between these two figures and therefore, the significant disagreement between the optimized solution shown in Figure 6 and the HK99 results presented in Figure 3 are not due to reduced water inflow via the Kara Gate.

[75] The second experiment shows that there are striking differences in circulation patterns of Figure 16b and Figure 6a. Without baroclinic effects, the circulation is driven by water fluxes via open boundaries because wind stresses are very small in summer. In this case, the major circulation flows are regulated by bathymetry and the Coriolis effect. The major flow from the Kara Gate follows the bathymetry and runs through the central Kara Sea toward Vilkitsky and Shokalsky straits. River runoffs from the Ob and Yenisey rivers join the major flow at 74°N and do not show any signs of the ROFI zone configuration. This circulation agrees better with the HK99 circulation pattern than with the control model run results. This confirms our conclusion that the HK99 underestimated horizontal gradients in the Kara Sea S fields.

[76] These conclusions explain the absence of the ROFI zone in the NPS-18 model results. The major problems of the NPS-18 model, at least for the Kara Sea, is that all boundaries of this regional Arctic model are closed and therefore there are no direct water volume fluxes to the sea from river deltas. This situation leads to the underestimation of the role of river runoff in the marginal seas, smoothing of water mass fronts, and reduction of vertical water stratification. These also result in the decrease of upper layer T and increase of upper layer salinities. The vertical model resolution is too coarse and does not resolve well the bathymetry, halocline and thermocline structures in the marginal seas.

[77] The specific problem of the Kara Sea circulation reproduced by the NPS-18 model is a flow from the Laptev

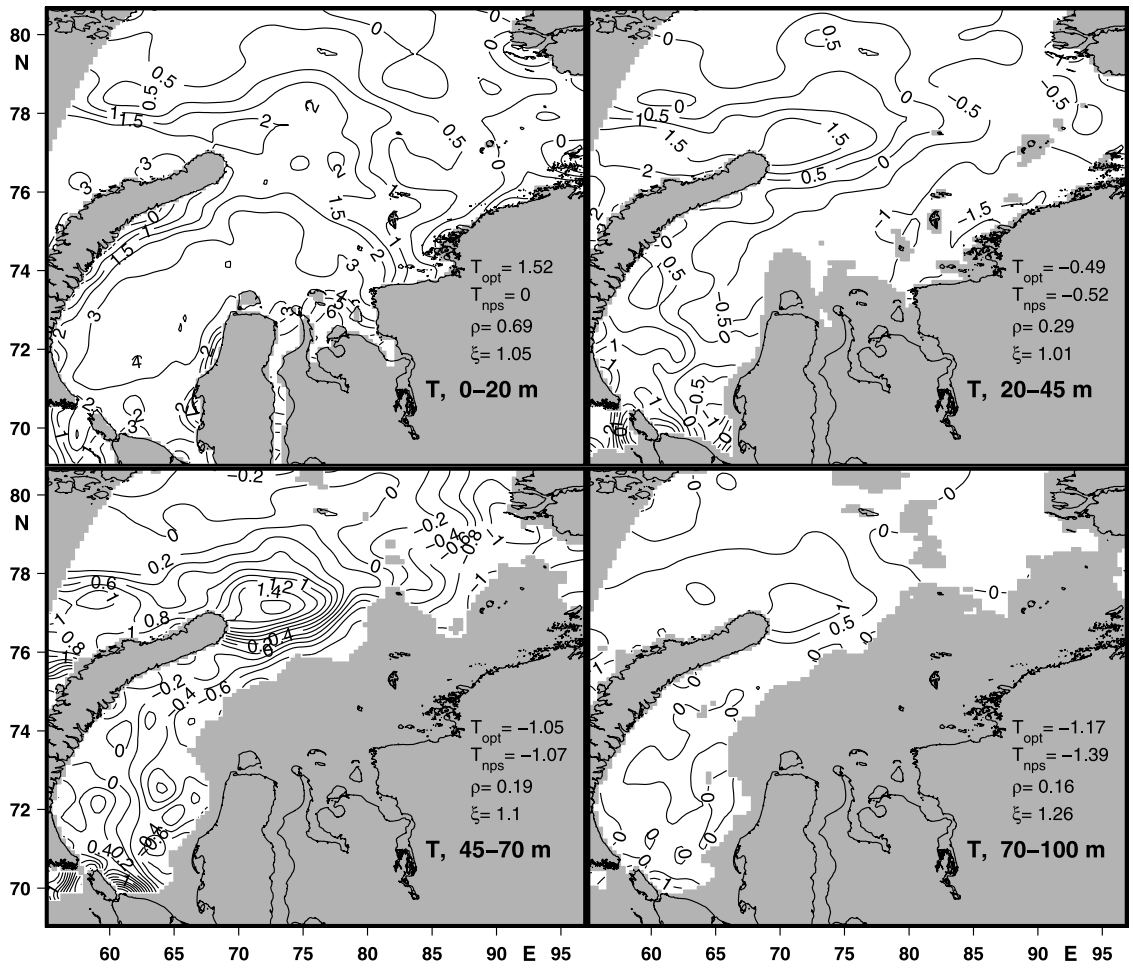

Figure 13. Temperature differences between the reconstructed Kara Sea fields and NPS-18 model results for the layers 0–20 m (a), 20–45 m (b), 45–70 m (c), and 70–100 m (d). T_{opt} and T_{nps} are the mean values of the reconstructed and NPS-18 fields. The correlation coefficients (ρ) and relative errors (ξ) between the mean reconstructed fields and NPS-18 fields are calculated for each layer.

Sea to the Kara Sea via Vilkitsky Strait. Numerous previous studies and observational data show that there is a current from the Kara Sea to the Laptev Sea, and biological studies also confirm this indicating a high abundance of Kara Sea foraminifera in the western part of the Laptev Sea [*Lukina*, 2001].

5.2. Circulation Change Under Arctic Oscillation

[78] The employed quasi-stationary approach can be easily modified and applied for the reconstruction of the monthly evolution of the Kara Sea circulation [e.g., *Nechaev et al.*, 2005; *Panteleev et al.*, 2006a]. This would allow an investigation not only of the circulation patterns and their variability in the region, but also a validation of the different numerical models against more accurate data fields obtained by the data assimilation techniques. Unfortunately, the sparseness of the monthly T and S data does not allow us to reconstruct the monthly evolution of the Kara Sea circulation. But in these final remarks, we consider changes of the Kara Sea circulation associated with different phases of the Arctic Oscillation (AO) index and show water circulation patterns for the years with positive (AO+) and negative phases (AO–) of the AO.

[79] The 6-hourly wind stresses for August and September were calculated from NCAR/NCEP reanalysis sea level pressure fields and averaged to force our model for the years with the highest (1967, 1975, 1989, 1990, and 1992) and lowest (1958, 1960, 1966, 1969, 1980, 1985) AO index years. The obtained wind stress fields are shown in Figures 5b and 5c. Note that the wind stress distribution during the AO– phase is rather similar to the climatological August–September wind stress pattern, while AO+ wind stresses differ significantly from the typical climatological distribution.

[80] The summer observations of T and S during the years mentioned above were extracted from the AARI hydrographic database and *NOAA* [2004]. The Ob/Yenisey discharges were defined as 0.015/0.015 Sv and 0.02/.015 Sv during the period of AO+ and AO–, respectively (http://www.R-ArcticNET.sr.unh.edu). Due to the lack of other measurements, the climatological transports through the western boundaries discussed earlier were assimilated.

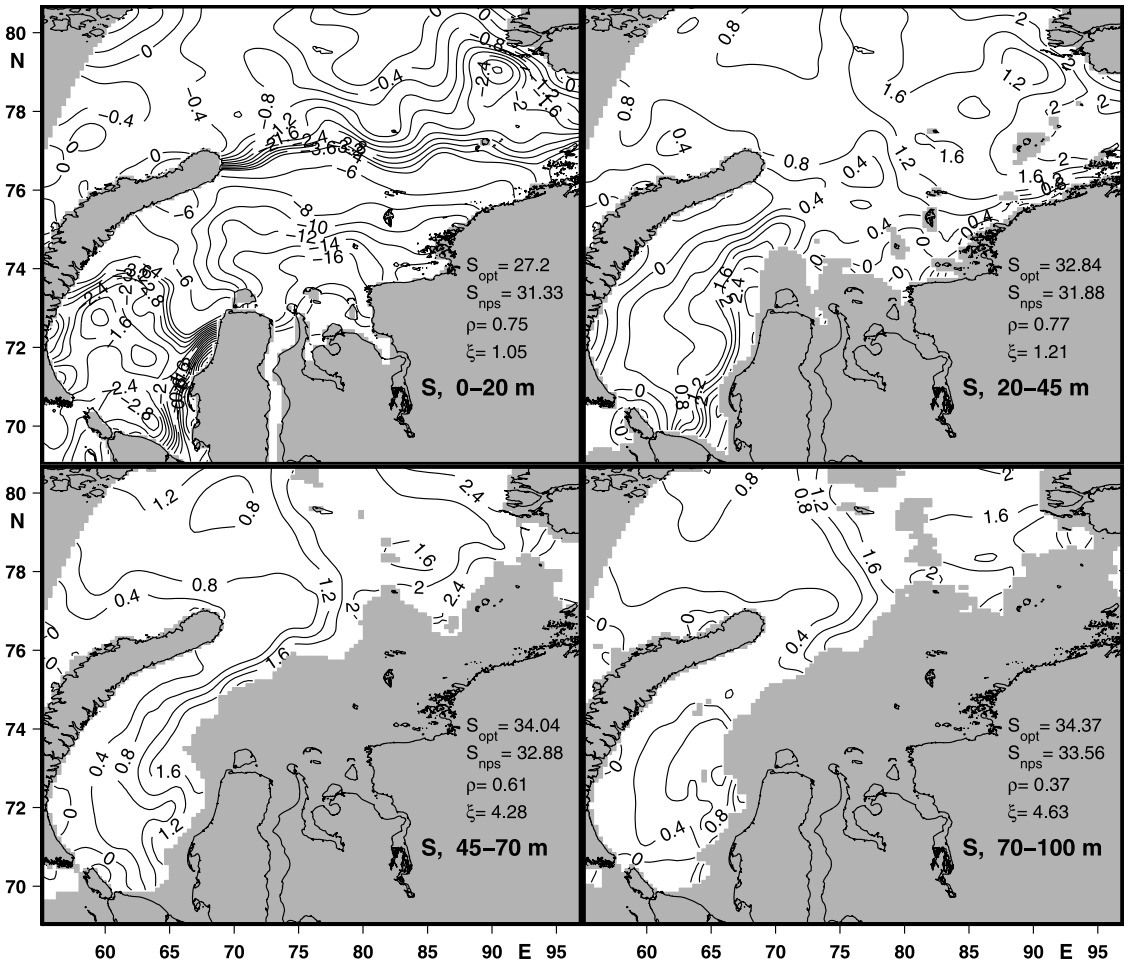

Figure 14. Salinity differences between the reconstructed Kara Sea fields and NPS-18 model results for the layers 0–20 m (a), 20–45 m (b), 45–70 m (c), and 70–100 m (d). S_{opt} and S_{nps} are the mean values of the reconstructed and NPS-18 fields. The correlation coefficients (ρ) and relative errors (ξ) between the mean reconstructed fields and NPS-18 fields are calculated for each layer.

Because of the sparseness of T and S data and uncertain transports along the western and other boundaries, the northern regions were excluded from consideration and only qualitative comparisons between the near-surface Kara Sea circulation during the periods of the AO+ and AO− are provided.

[81] The optimized AO+ and AO− T, S and velocity fields at 12.5 m are shown in Figure 17 and reveal at least three distinct features: (i) during the AO+ phase, the T in Kara Gate and in the southern part of the NZT is approximately 1.5°–3°C higher than during the AO− phase; (ii) during the AO− phase the warm water is accumulated near the northern tip of NZ. This process leads to the formation of a bulge of warm water that is absent during the AO+ phase; (iii) during the AO+ phase the ROFI zone is shifted approximately 200 km eastward.

[82] These features of the AO+ state agree with the domination of the southwest AO+ wind stresses (Figure 5b). We speculate that the AO+ southwest and western winds over the Barents and Kara seas push the surface waters on-shore and increase the eastward transport of the warm water through the Kara Gate. Our results indicate a small 0.1 Sv increase of the eastward Kara Gate transport during the AO+ phase. The real difference between Kara Gate transport for AO− and AO+ years can be even larger, because the mean climatological value of Kara Gate transport was assimilated in both cases due to the lack of the other data. A similar influence of the wind stresses on the inflow of the Atlantic water into the Barents Sea was observed by *Ingvaldsen et al.* [2004].

[83] Because of southwest winds, the whole system of the NZT circulation is shifted eastward during the AO+ years. As a result, the southwestward current along the east coast of NZ is stronger, and the northeastward flow along the NZT is localized along the 100 m isobath of the eastern flank of the NZT. Similarly, the current along the western NZ coast does not deflect to the north near the northern tip of NZ but continues to flow eastward. During the AO+ phase these two currents join near the northern tip of NZ and flow eastward as a broad current, while in the mean summer climatological state (Figure 6) and in the AO− state (Figure 17f), these currents diverge and there is a distinct region with weak currents and warm water between them.

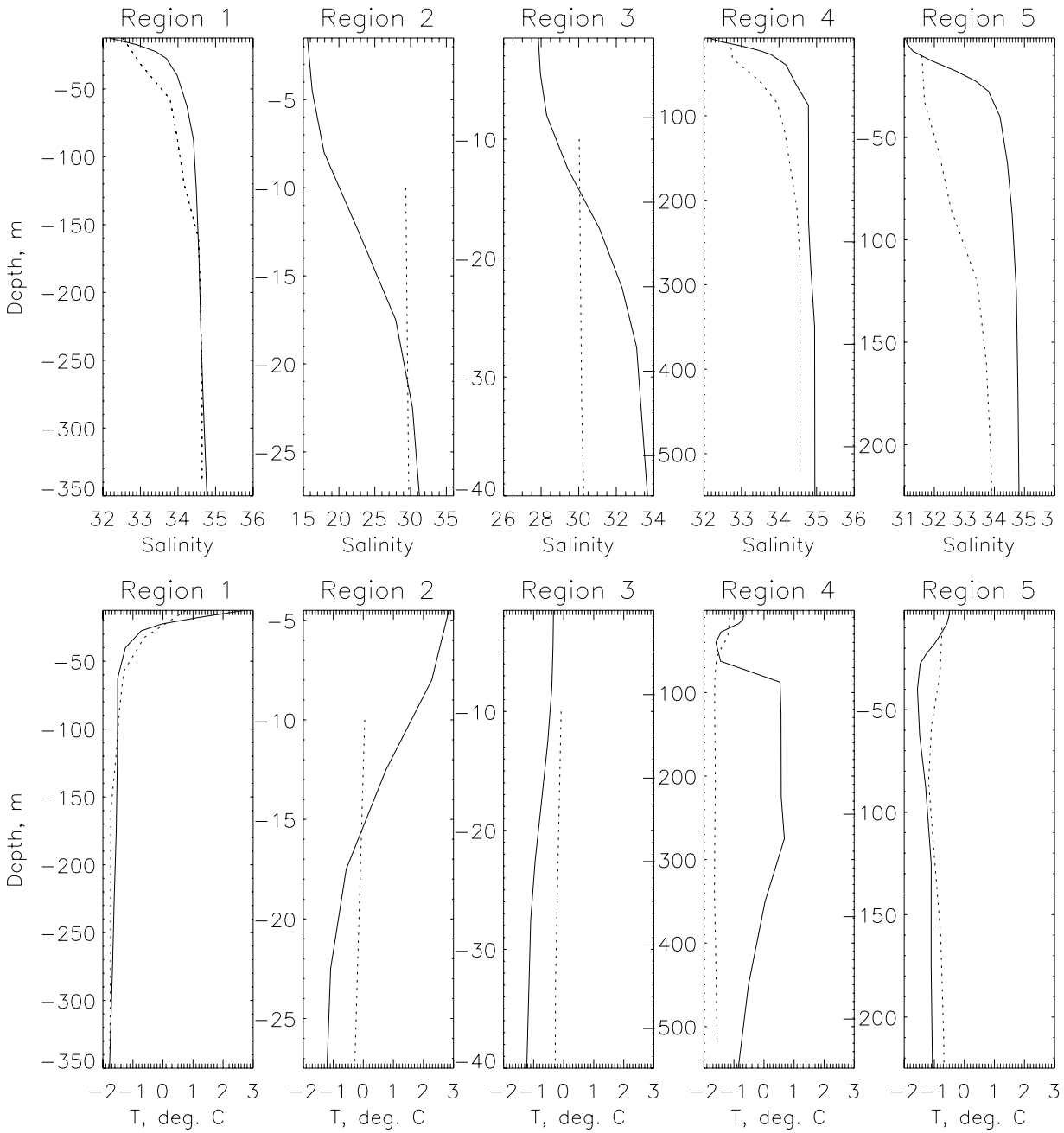

Figure 15. Typical T and S vertical profiles for five regions of the Kara Sea. Solid lines represent reconstructed data, and dashed lines depict parameters from the NPS-18 model results.

[84] Comparing Figures 17e and 17f, the western AO+ winds (Figure 6b) cause the increase of the onshore transport in the northern part of the KS. That weakens the westward Persey Current along the FJL and intensifies the eastward current along the Severnaya Zemlya. Another effect of the AO+ winds is a change of the circulation in the ROFI zone. Figures 17e and 17f indicate significant weakening of the the westward current along the Siberian coast during the AO+ phase resulting in a moderate (0.18 Sv) increase of the total eastward transport through the eastern boundary. The weakening of the coastal current also results in the decrease of the intrusion of the salt water into the Yenisey Bay during the AO+ phase. This phenomenon was modeled by *Harms et al.* [2003].

[85] The water transports through 13 sections for the AO+ and AO− phases are shown in Table 2. The AO+ and AO− solutions were obtained by assimilation of the relatively sparse T and S data. These results could be inaccurate and should be used only for the qualitative comparison between the two states.

[86] The climatological freshwater content calculated relative to reference salinity 34.80 ppt in the layer 0–100 m is approximately 4300 km^3. Our results indicate that the total freshwater storage varies by 3% between AO− (4280 km^3) and AO+ (4410 km^3). These absolute values and variability range are consistent with the estimates of *Proshutinsky et al.* [2006]. Recently, *Steele and Ermold* [2004] analyzed salinity trends in the Siberian shelves and speculate that during

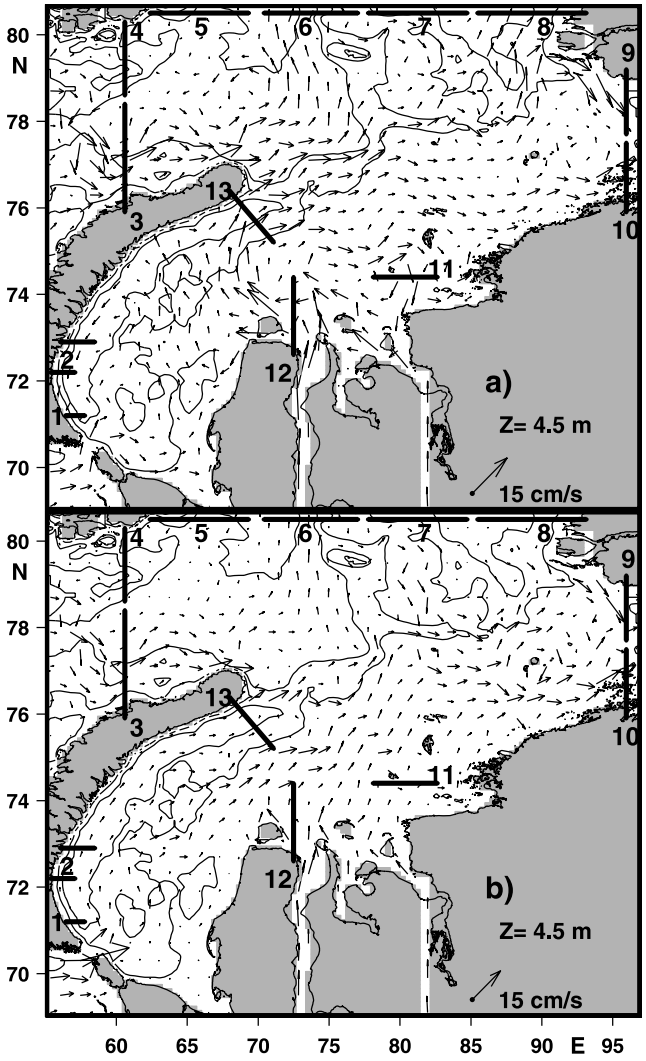

Figure 16. Circulation patterns at 4.5 m level for two numerical experiments. (top) Vectors representing results of experiment 1 when water transport via the Kara Gate was reduced to 0.2 SV and corresponded to water transport used in HK99 model. (bottom) Results of experiment 2 when water transport via all boundaries corresponded to the control model run but water T and S were uniform in vertical and horizontal directions reproducing a pure barotropic circulation forcing regime.

the high AO index freshwater export from the Kara Sea is significantly higher than the freshwater export during the low AO index. Our results show approximately a 20% difference between of AO+ and AO− freshwater flux from the Kara Sea. Interestingly, the changes in the freshwater flux through the Vilkitsky/Shokalsky contribute almost 70% of the interdecadal variability in the Kara Sea.

6. Summary

[87] 1. The Kara Sea summer climatologic water circulation is reconstructed employing a variational optimization of the initial and boundary conditions (climatology) of a 3-D quasi-stationary ocean circulation model adapted for this marginal sea of the Arctic Ocean. The circulation is characterized by inflows of 0.63 Sv via the Kara Gate and 1.18 Sv through the FJL-NZ passage. About 80% of the Kara Gate water crosses the entire sea and flows to the Laptev Sea via the Vilkitsky and Shokalsky Straits. The rest of the Kara Gate inflow goes through the Voronin Trough. The water inflow detected between the FJL and NZ outflows through the St. Anna Trough.

[88] 2. In general, the optimized surface circulation pattern is in agreement with a classic cyclonic circulation scheme of *Soviet Arctic* [1970], but disagrees in details and especially in the central part of the Kara Sea. In this so called ROFI zone, the reconstructed dynamics reveals a strong closed anticyclonic circulation associated with river runoff. This anticyclonic circulation is a prominent feature of the Kara Sea dynamics in summer and its observational evidence was provided by ADCP velocity measurements [*King et al.*, 1996]. Similar results were also obtained by McC00 with their Kara Sea laboratory model.

[89] 3. Reanalysis of the KS circulation during positive and negative Arctic Oscillation phases reveals a significant variability (up to 30%) in water transports via the open boundaries indicating and confirming that the wind forcing plays an important role in the Kara Sea water dynamics. This factor is also responsible to some degree for the interdecadal variability of the Kara Sea freshwater content which changes from positive to negative AO phase, is maximal in the upper 100 m layer and reaches 3% of the climatologic freshwater content in the region (which is 4300 km^3). This is in agreement with the estimates of the interannual variability of freshwater content in the entire Arctic Ocean [*Proshutinsky et al.*, 2006]. They found that the seasonal change of freshwater content is approximately 15% and the interdecadal change is also 3% or approximately 2,100 km^3 from the total Arctic Ocean freshwater content of 70,000 km^3. The Kara Sea is one of the major sources of fresh water to the Arctic Ocean (ca. 940 km^3 per year) due to the Ob and Yenisei river discharges and, depending on wind regime or prevailing climate state, this water could be accumulated by the sea or go directly to the arctic basin. Air-sea-ice interactions regulates the vertical water stratification in the upper layers of the Arctic Ocean [*Steele and Boyd*, 1998; *Steele and Ermold*, 2004] and influences the Arctic Ocean thermal regime via the heat exchange between the ocean ice and atmosphere.

[90] 4. Another implication of the reconstructed circulation patterns is their importance for biological studies and for assessing the transport of pollutants from Ob and Yenisei rivers and other sources of different contaminants in this region [*AMAP*, 1998].

[91] 5. Some outputs from a laboratory model and two numerical models of the Kara Sea were validated against optimized hydrography and circulation patterns obtained in this study. The validation results allow us to conclude that:

[92] (a) The laboratory McC00 model circulation scheme agrees with reconstructed currents very well. Unfortunately the quantitative comparison between our and McC00 results is not straightforward due to differences in the model domains and approaches.

[93] (b) The results of HAMSOM regional numerical model reveal several differences with the optimized circu-

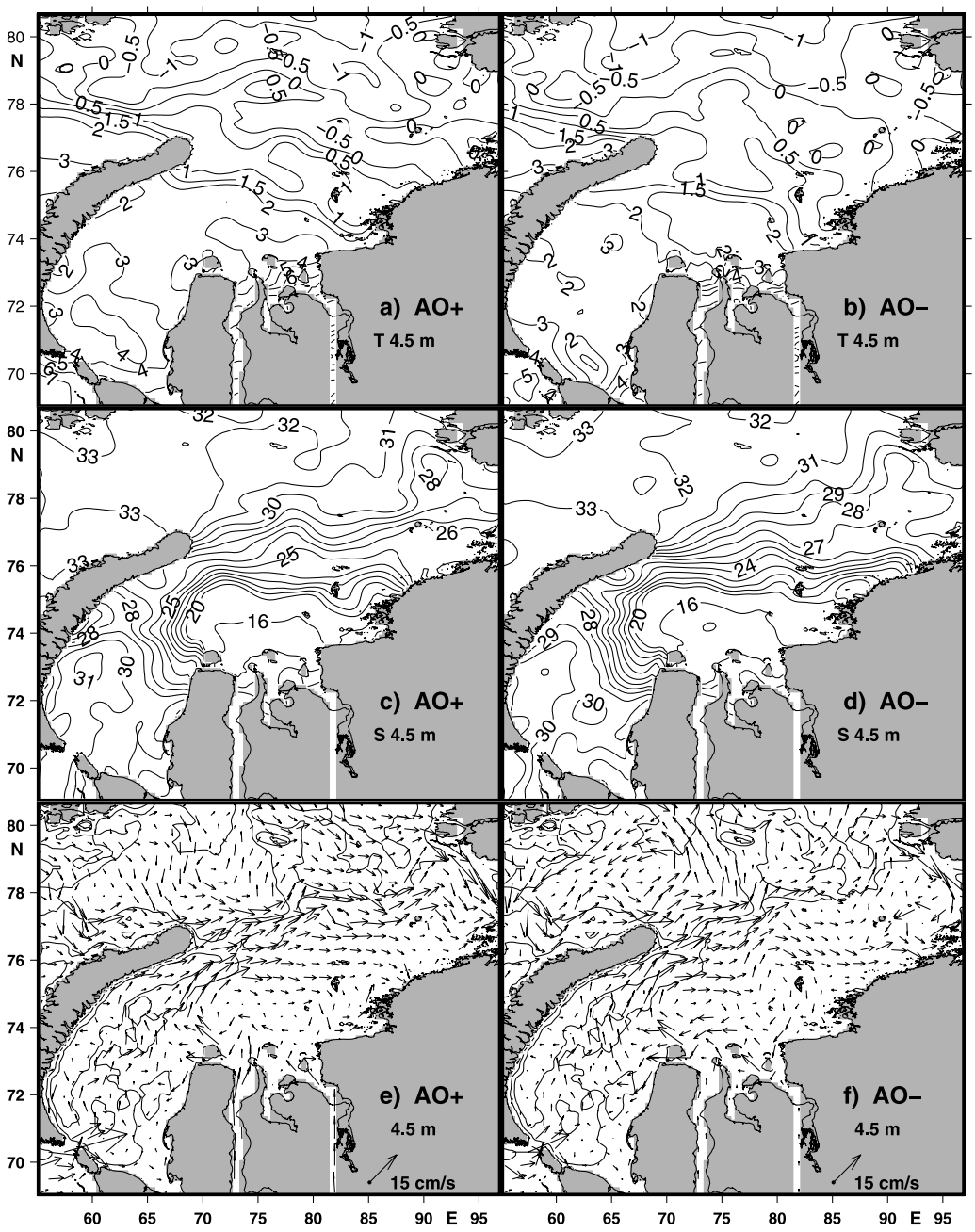

Figure 17. Hydrography and circulation of the Kara Sea reconstructed for periods of AO+ and AO−. (a, c, e) Water T, S and circulation patterns for AO+. (b, d, f) Water T, S and circulation patterns for AO−.

lation, which are probably due to the underestimation of the freshening of the Kara Sea discussed by HK99.

[94] (c) The results of the NPS-18 Arctic Ocean model differ significantly from the available observations and from optimized solutions. We can speculate that the major problem of this model (at least in the Kara Sea region) is an implicit description of rivers discharge. The vertical

Table 2. Transport (Sv) Through the 13 Sections at Figure 7 in the Optimized Climatological Kara Sea Solution, in the Optimized Solution During AO+ and AO−, and in the Experiments A and B

State	(1)	(2)	(3)	(4)	(5)	(6)	(7)	(8)	(9)	(10)	(11)	(12)	(13)
Clim.	0.07	0.13	1.39	−0.21	−0.44	1.61	−0.07	0.22	0.37	0.15	−0.08	−0.09	0.75
AO+	−0.02	0.06	1.03	0.07	−0.09	1.30	−0.09	0.13	0.49	0.21	−0.06	−0.09	0.90
AO−	0.02	0.10	1.90	−0.78	−0.29	1.38	−0.04	0.09	0.40	0.11	−0.07	−0.09	0.85
Exp. A	0.01	0.04	1.41	−0.07	−0.19	1.41	−0.04	0.11	0.16	0.12	−0.06	−0.07	0.47
Exp. B	0.05	0.15	1.23	−0.11	−0.15	1.29	−0.06	0.15	0.37	0.22	0.03	0.	0.5

model resolution is also rather coarse and does not resolve well the bottom topography and vertical water stratification.

[95] 6. The data assimilation approach has some advantages compared with the conventional methods of ocean state analysis based on geostrophic balance or more complex traditional methods of numerical modeling without data assimilation.

[96] The major advantage of the reconstructed circulation is that it is reasonably close to the existing data, and at the same time, all reconstructed fields (T, S, velocity, surface heat/salt and momentum fluxes) are dynamically balanced.

[97] **Acknowledgments.** This research is supported by the Frontier Research System for Global Change, through JAMSTEC, Japan, and by the National Science Foundation Office of Polar Programs (under cooperative agreements OPP-0002239 and OPP-0327664 with the International Arctic Research Center, University of Alaska Fairbanks). The development of the data assimilation system, utilized in this study, was also supported by NSF grant OCE-0118200.

References

AMAP (1998), AMAP assessment report: Arctic pollution issues, Arctic Monitoring and Assessment Program (AMAP), xii+859 pp., Oslo, Norway.

Awaji, T., S. Masuda, Y. Ishikawa, N. Sugiura, T. Toyoda, and T. Nakamura (2003), State estimation of the North Pacific Ocean by a four-dimensional variational data assimilation experiment, *J. Oceanogr.*, *59*, 931–943.

Backhaus, J. O. (1985), A three-dimensional model for the simulation of shelf sea dynamics, *Dsch. Hydrogr. Z.*, *38*(H4), 165–187.

Berezkin, V. A. and G. Y. Ratmanov (1940), A general scheme of currents of the Arctic Ocean and adjacent seas, in *Hydrograpic Administration of the Navy* (in Russian), 10 pp., Leningrad.

DaSilva, A., C. C. Young, and S. Levitus (1995), Atlas of Surface Marine Data, NOAA Atlas NESDIS 6, Natl. Oceanogr. Data Cent., Silver Spring, Md.

Doronin, N. Y. (1983), Simulation of the barotropic circulation in the Kara Sea (in Russian), *Trans. Arct. Antarct. Res. Inst.*, *380*, 54–62.

Doronin, N. Y. (1987), Diagnostic calculation of the three-dimensional circulation in the Kara Sea (in Russian), *Problems Arct. Antarct.*, *63*, 47–53.

Doronin, N. Y., V. L. Kuznetcov, and A. Y. Proshutinsky (1991), Circulation of the water masses in the Kara Sea, *Trans. Arct. Antarct. Res. Inst.*, *424*, 34–41.

Gilbert, J. C., and C. Lemarechal (1989), Some numerical experiments with variable storage quasi-Newton algorithms, *Math. Prog.*, *45*, 407–455.

Grotov, A. S., D. A. Nechaev, G. G. Panteleev, and M. I. Yaremchuk (1998), Circulation in Bellingshausen and Amundsen Seas, *J. Geophys. Res.*, *103*, 13,011–13,023.

Harms, I. H., and M. J. Karcher (1999), Modeling the seasonal variability of hydrography and circulation in the Kara Sea, *J. Geophys. Res.*, *104*(C6), 13,431–13,448.

Harms, I. H., and M. J. Karcher (2005), Kara Sea freshwater dispersion and export in the late 1990s, *J. Geophys. Res.*, *110*, C08007, doi:10.1029/2004JC002744.

Harms, I. H., U. Huebner, J. Backhaus, M. Kulakov, V. Stanovoy, O. Stepanets, L. Kodina, and R. Schlitzer (2003), Salt intrusions in Siberian River Estuaries: Observations and model experiments for Ob and Yenisei, *Proc. Mar. Sci.*, *6*, 47–72.

Hibler, W. D., III (1979), A dynamic thermodynamic sea ice model, *J. Phys. Oceanogr.*, *9*, 815–846.

Ingvaldsen, R., L. Asplin, and H. Loeng (2004), Velocity field of the western entrance to the Barents Sea, *J. Geophys. Res.*, *109*, C03021, doi:10.1029/2003JC001811.

Karcher, M. J., M. Kulakov, S. Pivovarov, U. Schauer, F. Kauker, and R. Schlitzer (2003), Atlantic Water flow to the Kara Sea: Comparing model results with observations, in *Siberian River Run-Off in the Kara Sea*, edited by R. Stein, K. Fahl, E. M. Galimov, and O. V. Stepanets, Elsevier, New York.

King, S. E., D. R. Johnson, and J. Carroll (1996), EPOCA-95 cruise report, *Rep. NRL/MR/6616-96-7813*, 51 pp., Nav. Res. Lab., Washington, D. C.

Kulakov, M. and V. Stanovoi (2002), Frontal zones in the Kara Sea: Observation and modeling, paper presented at 11th International Niennial Conference on Physics of Estuaries and Coastal Zones, Hamburg, Germany, 17–20 Sept.

Le Dimet, F. X., and O. Talagrand (1986), Variational algorithms for analysis and assimilation of meteorological observations: Theoretical aspects, *Tellus, Ser. A*, *38*, 97–100.

Loeng, H., V. Ozhigin, R. Adlansvik, and H. Sagen (1993), Current measurements in the northeastern Barents Sea, paper presented at ICES Statutory Meeting, Dublin.

Loeng, H., V. Ozhigin, and B. Adlansvik (1997), Water fluxes through the Barents Sea, *ICES J. Mar. Sci.*, *54*, 310–317.

Lukina, T. G. (2001), Foraminifera of the Laptev Sea, *Protistology*, *2*(2), 105–122.

Madec, G., P. Delecluse, M. Imbard, and C. Levy (1999), OPA8.1 Ocean General Circulation Model: Reference Manual, Note du Pole modelisation, 91 pp., Inst. Pierre-Simon Laplace (IPSL), Paris, France.

Marchuk, G. I. (1974), Basic and adjoint equation of the ocean and atmosphere dynamic, *Meteorol.*, 17–34.

McClimans, T. A., D. R. Johnson, M. Krosshavn, E. E. King, J. Carroll, and O. Grenness (2000), Transport processes in the Kara Sea, *J. Geophys. Res.*, *105*(C6), 14,121–14,139.

Nechaev, D. A., G. G. Panteleev, and M. I. Yaremchuk (2005), Reconstruction of the circulation in the limited region with open boundaries: Circulation in the Tsushima Strait, *Okeanologiya*, *45*(6), 805–828.

NOAA (2004), Atlas NESDIS 58, Natl. Oceanogr. Data Cent., Silver Spring, Md.

Panteleev, G., M. Ikeda, A. Grotov, D. Nechaev, and M. Yaremchuk (2004), Mass, heat and salt balances in the eastern Barents Sea obtained by inversion of a hydrographic section data, *J. Oceanogr.*, *60*, 613–623.

Panteleev, G. G., D. A. Nechaev, and M. Ikeda (2006a), Reconstruction of summer Barents Sea circulation from climatological data, *Atmos. Ocean*, *44*(2), 111–132.

Panteleev, G. G., P. Stabeno, V. A. Luchin, D. A. Nechaev, and M. Ikeda (2006b), Summer transport estimates of the Kamchatka Current derived as a variational inverse of hydrophysical and surface drifter data, *Geophys. Res. Lett.*, *33*, L09609, doi:10.1029/2005GL024974.

Parkinson, C. L., and W. M. Washington (1979), A large scale numerical model of sea ice, *J. Geophys. Res.*, *84*, 311–337.

Pavlov, V. K., and S. I. Pfirman (1995), Hydrographic structure and variability of the Kara Sea: Implication for pollutant distribution, *Deep Sea Res., Part II*, *42*, 1369–1390.

Penenko, V. V. (1981), *Methods of Numerical Simulation of Atmospheric Processes*, 347 pp., Hydrometeoizdat, St. Petersburg, Russia.

Pivovarov, S., R. Schlitzer, and A. Novikhin (2003), River run-off influence on the water mass formation in the Kara Sea, *Proc. Mar. Sci.*, *6*, 9–26.

Potanin, V. A. and S. V. Korotkov (1988), Seasonal variability of the main currents in the southern Barents Sea and water exchange with the adjacent areas, in *Geological and Geographical Problems of Natural Resources Exploitation in the Northern Seas* (in Russian), pp. 81–90, Murmansk.

Proshutinsky, A., R. Krishfield, E. Carmack, F. McLaughlin, and K. Shimada (2006), Investigation of the Beaufort Gyre freshwater reservoir and its role in Arctic climate variability, *Eos Trans. AGU*, *87*(36), Ocean Sci. Meet. Suppl., Abstract OS45H-03.

Scherbinin, A. (2001), Measurements in the Kara strait, in *Experience of System Oceanologic Studies in the Arctic*, pp. 128–133, Sci. World, Moscow.

Smith, R. D., J. K. Dukowicz, and R. C. Malone (1992), Parallel ocean general circulation modeling, *Physica D*, *60*, 38–61.

Soviet Arctic (1970), *Seas and Islands of the Arctic Ocean* (in Russian), 526 pp., Nauka, Moscow.

Stammer, D., C. Wunsch, R. Giering, C. Eckert, P. Heimbach, J. Marotzke, A. Adcroft, C. N. Hill, and J. Marshal (2002), Global circulation during 1992–1997, estimated from ocean observations and a general circulation model, *J. Geophys. Res.*, *107*(C9), 3118, doi:10.1029/2001JC000888.

Steele, M., and T. Boyd (1998), Retreat of the cold halocline layer in the Arctic Ocean, *J. Geophys. Res.*, *103*(C5), 10,419–10,436.

Steele, M., and W. Ermold (2004), Salinity trends on the Siberian Shelves, *Geophys. Res. Lett.*, *31*, L24308, doi:10.1029/2004GL021302.

Thacker, W. C. (1989), The role of the Hessian matrix in fitting models to measurements, *J. Geophys. Res.*, *94*(C5), 6177–6196.

Thacker, W. C., and R. Long (1988), Fitting dynamics to data, *J. Geophys. Res.*, *93*, 10,655–10,665.

Timofeyev, V. T. (1963), Interaction of Arctic Ocean water with the Atlantic and Pacific waters (in Russian), *Oceanography*, *3*, 569–578.

Turanov, I. (1963), Water exhange through the Arctic Straits (an overview of the present studies) (in Russian), *Sci. Res. Proj. OK-9/3*, 100 pp., Arct. and Antarct. Res. Inst. Arch., Leningrad.

Tziperman, E., and W. C. Thacker (1989), An optimal-control/adjoint equation approach to studying the oceanic general circulation, *J. Phys. Oceanogr.*, *19*, 1471–1485.

Uralov, N. S. (1960), On the advective component of the heat balance in the southern Barents Sea (in Russian), *Trudy Gosudarstvennogo Oceanogr. Inst.*, *55*, 3–20.

Volkov, V. A., O. M. Johannessen, V. E. Boradachev, G. N. Voinov, L. H. Pettersson, L. P. Bobylev, and A. V. Kouraev (2002), *Polar Seas Oceanography: An Integrated Case Study of the Kara Sea*, Springer, New York.

Wunsch, C. (1994), Dynamically consistent hydrography and absolute velocity in the eastern North Atlantic Ocean, *J. Geophys. Res.*, *99*(C7), 14,071–14,090.

Wunsch, C. (1996), *The Ocean Circulation Inverse Problem*, 442 pp., Cambridge Univ. Press, New York.

Yaremchuk, M. I., D. A. Nechaev, J. Schroeter, and E. Fahrbach (1998), A dynamically consistent analysis of circulation and transports in the southwestern Weddell Sea, *Ann. Geophys.*, *16*, 1024–1038.

Zhang, Y., W. Maslowski, and A. J. Semtner (1999), Impact of mesoscale ocean currents on sea ice in high-resolution Arctic ice and ocean simulations, *J. Geophys. Res.*, *104*, 18,409–18,429.

M. Kulakov, Arctic and Antarctic Research Institute, 199397 St. Petersburg, Russia.

W. Maslowski, Department of Oceanography, Naval Postgraduate School, Monterey, CA 93943-5122, USA.

D. A. Nechaev, Department of Marine Science, University of Southern Mississippi, Stennis Space Center, MS 39529, USA.

G. Panteleev, International Arctic Research Center, University of Alaska Fairbanks, Fairbanks, AK 99775-7335, USA. (gleb@iarc.uaf.edu)

A. Proshutinsky, Woods Hole Oceanographic Institution, Woods Hole, MA 02543, USA.